Virginia Center *for* Transportation
INNOVATION & RESEARCH

Structural Design Guidelines for Concrete Bridge Decks Reinforced With Corrosion-Resistant Reinforcing Bars

http://www.virginiadot.org/vtrc/main/online_reports/pdf/15-r10.pdf

ABRAHAM LAMA SALOMON
Graduate Research Assistant

CRISTOPHER D. MOEN, Ph.D., P.E.
Associate Professor

The Charles E. Via, Jr. Department of Civil and Environmental Engineering

Virginia Polytechnic and State University

Final Report VCTIR 15-R10

VIRGINIA CENTER FOR TRANSPORTATION INNOVATION AND RESEARCH
530 Edgemont Road, Charlottesville, VA 22903-2454
www.VTRC.net

Standard Title Page - Report on Federally Funded Project

1. Report No.: FHWA/VCTIR 15-R10	2. Government Accession No.:	3. Recipient's Catalog No.:
4. Title and Subtitle: Structural Design Guidelines for Concrete Bridge Decks Reinforced with Corrosion-Resistant Reinforcing Bars		Report Date: October 2014
		6. Performing Organization Code:
7. Author(s): Abraham Lama Salomon, and Cristopher D. Moen, Ph.D., P.E.		8. Performing Organization Report No.: VCTIR 15-R10
9. Performing Organization and Address: Virginia Center for Transportation Innovation and Research 530 Edgemont Road Charlottesville, VA 22903		10. Work Unit No. (TRAIS):
		11. Contract or Grant No.: 101602
12. Sponsoring Agencies' Name and Address: Virginia Department of Transportation 1401 E. Broad Street Richmond, VA 23219 / Federal Highway Administration 400 North 8th Street, Room 750 Richmond, VA 23219-4825		13. Type of Report and Period Covered: Final Contract
		14. Sponsoring Agency Code:
15. Supplementary Notes:		

16. Abstract:

This research program develops and validates structural design guidelines and details for concrete bridge decks with corrosion-resistant reinforcing (CRR) bars. A two-phase experimental program was conducted where a control test set consistent with a typical Virginia Department of Transportation bridge deck design using Grade 60 steel (ASTM A615, f_y = 60 ksi) and epoxy-coated reinforcing steel was compared to deck slab specimens where Grade 60 is replaced with CRR bars.

The experimental program was designed to evaluate how flexural performance at service and ultimate limit states are affected by a one-to-one replacement of Grade 60 with CRR bars, a reduction of concrete clear cover, and a reduction in rebar size. Structural analysis models were developed using Response 2000 in order to predict the CRR bridge deck moment-curvature and the moment-crack width relationships.

Experimental trends proved to be consistent with the analytical results demonstrating the viability of Response 2000 as a design tool for reinforced concrete with high-strength and nonmetallic rebar without a defined yield plateau. For reduced bar size and clear cover (2.00 in instead 2.50 in), ASTM A1035 and UNS S32304 specimens proved to have similar deformability ratios and crack widths that comply with current AASHTO requirements, with as much as 36% less steel.

17 Key Words: Bridge, Decks, Design, Model, Reinforcement, Steel, Structural	18. Distribution Statement: No restrictions. This document is available to the public through NTIS, Springfield, VA 22161.		
19. Security Classif. (of this report): Unclassified	20. Security Classif. (of this page): Unclassified	21. No. of Pages: 49	22. Price:

Form DOT F 1700.7 (8-72) Reproduction of completed page authorized

FINAL REPORT

STRUCTURAL DESIGN GUIDELINES FOR CONCRETE BRIDGE DECKS REINFORCED WITH CORROSION-RESISTANT REINFORCING BARS

Abraham Lama Salomon
Graduate Research Assistant

Cristopher D. Moen, Ph.D., P.E.
Associate Professor

The Charles E. Via, Jr. Department of Civil and Environmental Engineering
Virginia Polytechnic and State University

VCTIR Project Manager
Stephen R. Sharp, Ph.D., P.E.
Virginia Center for Transportation Innovation and Research

In Cooperation with the U.S. Department of Transportation
Federal Highway Administration

Virginia Center for Transportation Innovation and Research
(A partnership of the Virginia Department of Transportation
and the University of Virginia since 1948)

Charlottesville, Virginia

October 2014
VCTIR 15-R10

DISCLAIMER

The project that is the subject of this report was done under contract for the Virginia Department of Transportation, Virginia Center for Transportation Innovation and Research. The contents of this report reflect the views of the author(s), who is responsible for the facts and the accuracy of the data presented herein. The contents do not necessarily reflect the official views or policies of the Virginia Department of Transportation, the Commonwealth Transportation Board, or the Federal Highway Administration. This report does not constitute a standard, specification, or regulation. Any inclusion of manufacturer names, trade names, or trademarks is for identification purposes only and is not to be considered an endorsement.

Each contract report is peer reviewed and accepted for publication by staff of Virginia Center for Transportation Innovation and Research with expertise in related technical areas. Final editing and proofreading of the report are performed by the contractor.

ABSTRACT

This research program develops and validates structural design guidelines and details for concrete bridge decks with corrosion-resistant reinforcing (CRR) bars. A two-phase experimental program was conducted where a control test set consistent with a typical Virginia Department of Transportation bridge deck design using Grade 60 steel (ASTM A615, f_y = 60 ksi) and epoxy-coated reinforcing steel was compared to deck slab specimens where Grade 60 is replaced with CRR bars.

The experimental program was designed to evaluate how flexural performance at service and ultimate limit states are affected by a one-to-one replacement of Grade 60 with CRR bars, a reduction of concrete clear cover, and a reduction in rebar size. Structural analysis models were developed using Response 2000 in order to predict the CRR bridge deck moment-curvature and the moment-crack width relationships.

Experimental trends proved to be consistent with the analytical results demonstrating the viability of Response 2000 as a design tool for reinforced concrete with high-strength and nonmetallic rebar without a defined yield plateau. For reduced bar size and clear cover (2.00 in instead 2.50 in), ASTM A1035 and UNS S32304 specimens proved to have similar deformability ratios and crack widths that comply with current AASHTO requirements, with as much as 36% less steel.

FINAL REPORT

STRUCTURAL DESIGN GUIDELINES FOR CONCRETE BRIDGE DECKS REINFORCED WITH CORROSION-RESISTANT REINFORCING BARS

Abraham Lama Salomon
Graduate Research Assistant

Cristopher D. Moen, Ph.D., P.E.
Associate Professor

The Charles E. Via, Jr. Department of Civil and Environmental Engineering
Virginia Polytechnic and State University

INTRODUCTION

Extending design life and the need to reduce department of transportation maintenance costs are making corrosion-resistant reinforcing bars (CRR) an economically viable option for use in reinforced concrete bridges. Reinforcing steel corrosion is the leading cause of concrete deterioration in bridge deck slabs and marine structures, which reduces their service life and increases their life cycle cost. A wide variety of CRR options are available, including bars that meet ASTM A1035, ASTM A955, and AASHTO MP 13 requirements, all of which have improved corrosion resistance when compared to typical Grade 60 mild steels (Clemena et al., 2003; Ji et al., 2005). The same chemical compositions and manufacturing processes that provide corrosion resistance also change the steel's material properties, demonstrated with the highly variable CRR rebar tensile test results in Figure 1 (Sarver, 2010). With most CRRs, the steel stress-strain curve lacks a sharp yielding plateau. Steel yield stress and tensile rupture strength can increase by as much as two times that of typical grade 60 reinforcing steel bar. Elongation and post-yielding ductility may increase or decrease depending upon the material composition (see Figure 1). These material deviations from typical mild steel have mostly positive structural design implications, especially increased yield and ultimate strength.

The noticeable differences in CRR steel properties have yet to be used in U.S. bridge design. There are two primary reasons for this: (1) code provisions are based on strength and serviceability equations derived for concrete reinforced with Grade 60 mild reinforcement, and (2) existing concrete bridge systems, details, and dimensions are well established, making a shift to more efficient structural systems that fully utilize high performance materials a slow process.

A hurdle to structural design with CRR is that accurate, accessible methods for predicting flexural capacity, crack widths in service, and punching shear for bridge decks are not currently available. Experimental research does exist though that provides a glimpse of CRR's potential benefits. High-strength reinforcing steel arrived in the United States in the early 1960's with support from the Portland Cement Association (Hognestad et al., 1960). An experimental research project was initiated at Cornell University to evaluate the existing reinforced concrete

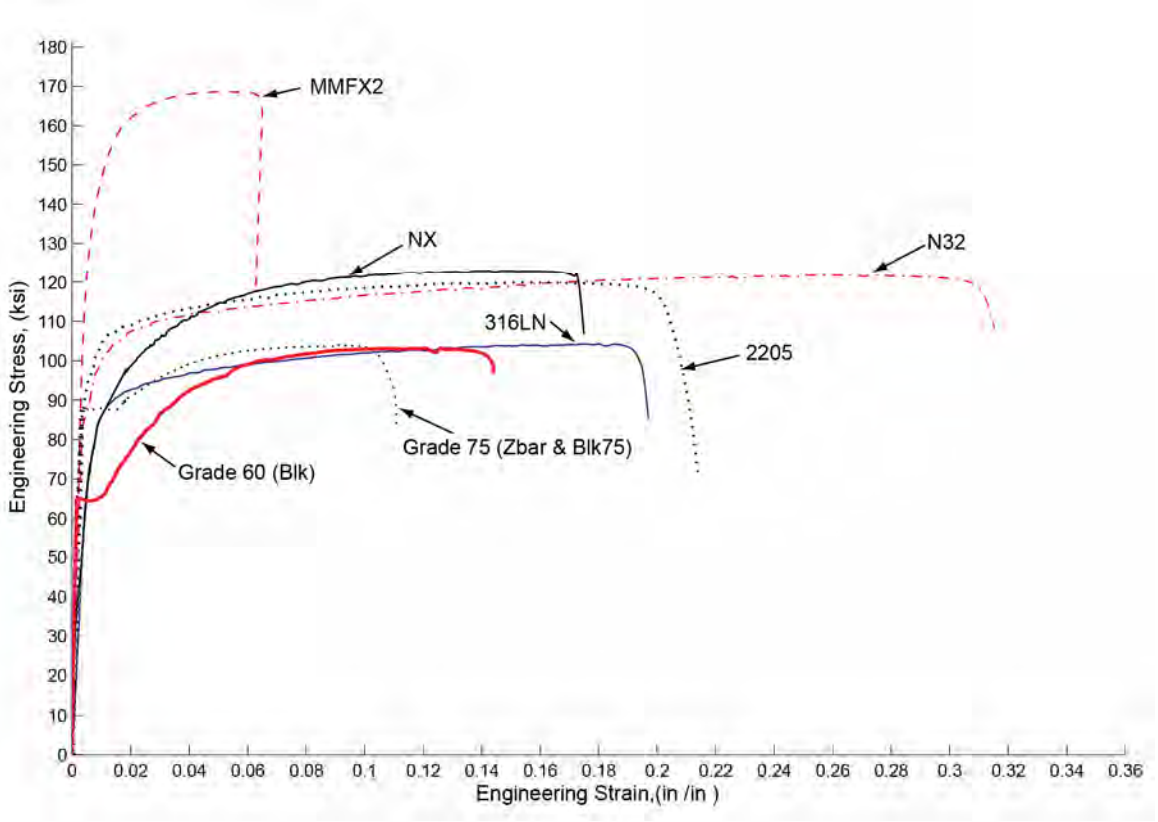

Figure 1. Corrosion Resistance Reinforcing Steel Stress-Strain Properties (Sarver, 2010)

capacity prediction method's validity for reinforcing concrete with high strength steels (Gurlanick, 1960). The research focused on the flexural capacity of T-beams reinforced with steel with yield stresses ranging from 83 to 103 ksi. Beam loading patterns were varied to study flexure or shear failures, and special care was taken to note crack width patterns at service and peak loads. The Cornell researchers observed that existing flexural strength predictions were conservative because of the elastic-plastic assumption implemented to address mild steel's sharp yielding plateau. High-strength steels exhibited gradual yielding behavior, accommodating increased flexural capacity through strain hardening without a sudden loss in stiffness. Even though higher tensile stresses existed in the high-strength steel at service loads, crack widths consistent with mild reinforcing were achieved by smaller, evenly spaced bars. Unfortunately, proposed changes to the existing (conservative) elastic-plastic strength prediction methods never evolved from this work, which delayed the introduction of concrete reinforced with high strength steels in the United States.

Interest in high-strength reinforcing steel reignited with the commercial development of ASTM A1035 reinforcing steel starting in 2002 (Malhas, 2002). The ASTM A1035 use was sought as a solution for corrosion resistance in bridge decks (Hartt et al., 2004) and rebar congestion relief in high-rise buildings (Faza et al., 2008). Research studies demonstrated ASTM A1035's structural viability, both in buildings (Yotakhong, 2003) and in bridge decks (Seliem et al., 2008). A direct one to one replacement of mild reinforcement (f_y=60 ksi) with

ASTM A1035 was shown to produce unfavorable compression zone failure modes in beams (Malhas, 2002). These results motivated increased allowable tensile strain limits to ensure a ductile failure with high-strength reinforcing steel (Mast et al., 2008; Shahrooz et al., 2010), and a cautious approach by AASHTO.

CRR can be used more efficiently in bridge decks if structural design and detailing hurdles are removed through new research. The NCHRP Project 12-77 (Report 679) on this topic initiated in 2007, providing an evaluation of the AASHTO Bridge Design Specifications concerning the use of reinforcing steel with no discernible yield plateau, including but not limited to high-strength reinforcing steel. This research builds on these NCHRP findings and the historical experimental record (e.g., the 1960s era Cornell studies) with the goal of preparing the Virginia Department of Transportation (VDOT) to implement CRR safely and efficiently in new bridge designs. The new knowledge provided by this project will allow the Virginia Department of Transportation to realize both short-term construction cost savings and improved long-term performance as they move toward broad CRR implementation in their concrete structures.

PURPOSE AND SCOPE

The research objective was to develop structural design guidelines, tools and details that accommodate CRR implementation in Virginia bridge decks. Of particular focus in this study was the relative flexural performance of bridge decks with CRR bars at service and ultimate limit states. Although not all of the CRR bars tested in this study are currently used by the Virginia Department of Transportation (VDOT), the bars tested all exhibited different behaviors when compared to Grade 60 reinforcement, which is of interest as VDOT continues to move forward in this area. The conclusions from this study will help VDOT implement design changes in bridge decks designed with the strip method, which assumes that the bridge deck acts as a one-way slab transversely between girders (AASHTO 2010). These changes will be reflected through updated design procedures, examples and tables in the VDOT Structures and Bridge Manual (VDOT 2011, Chapter 10).

A two-phase experimental program was conducted. In Phase I, flexural tests on one-way slabs, were performed to simulate negative transverse flexure over a bridge girder as assumed in the commonly used strip design method. Grade 60 (uncoated), epoxy-coated reinforcing Grade 60, UNS S24100 stainless steel (ASTM A955), UNS S32304 stainless steel (ASTM A955), ASTM A1035, and glass fiber–reinforced polymer (GFRP) bars that meet ACI 440.6-08 (ACI 2008) specifications were studied. The experimental program was designed to evaluate how flexural performance at service and ultimate limit states are affected by a one-to-one replacement of Grade 60 with CRR bars, a concrete top clear cover reduction, and a decrease in rebar size in the bridge deck top mat.

In Phase II, flexural tests were conducted similarly to Phase I using two layers of reinforcing bars (i.e. top and bottom). Grade 60 (uncoated), ASTM A1035, UNS S32304 stainless steel (ASTM A955), RockRebar^{TM} (BFRP) and carbon-fiber-reinforced polymer

(CFRP) bars that meet ACI 440.6-08 (ACI 2008) specifications were used in the study. The study objective is to investigate how concrete deck slabs flexural performance is affected by replacing the Grade 60 with CRR bars, while reducing the bar's diameter and the bottom clear cover. Also, specimens with only one layer of Grade 60 reinforcing bars were included in the analysis.

The test setup described in the following sections is designed to evaluate the flexural performance of a bridge deck's top reinforcing mat in tension, i.e., negative transverse flexure over a girder as shown in Figure 2.

This testing program also provides valuable data for validating computational reinforced concrete design tools, for example, the sectional analysis program Response 2000 (Bentz, 2000) originally developed for use with Grade 60 steel. The gradually yielding stress-strain curves common to CRR are incompatible with current elastic-plastic design equations. However, they can be directly input into Response 2000 to make flexural capacity, moment-curvature, and crack width predictions, thus avoiding the current need for a defined yield stress in design.

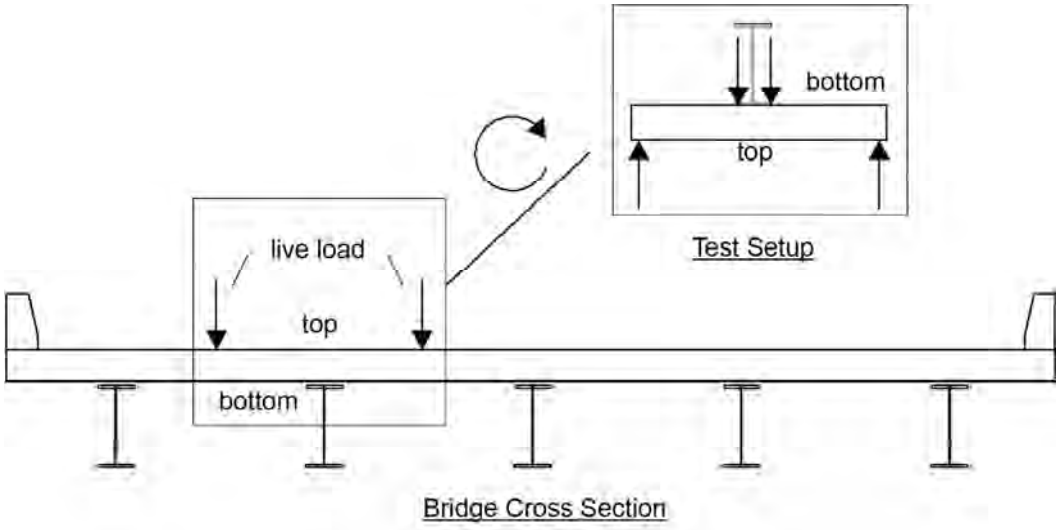

Figure 2. Experimental Program Designed to Test Bridge Deck Negative Flexure at a Girder

Methods

Experimental Variables and Test Matrix

The experimental strategy was to perform a control test group consistent with a typical VDOT bridge deck design using uncoated Grade 60 or Grade 60 epoxy-coated reinforcing (ECR), and then to compare these tests to specimens where the Grade 60 steel was replaced with CRR as summarized in Table 1 (Phase I) and Table 2 (Phase II). The goal of the control tests was to quantify how a typical concrete bridge deck design in Virginia is expected to perform at service and ultimate limit states.

Table 1. Phase I Test Matrix

Test Number	Bar Type	Bar Quantity	Clear Cover (in)	Reinforcement Ratio, ρ	Test Variable
1	Grade 60	No. 5 @ 6 in	2.50	0.009	Controls
2	Grade 60	No. 5 @ 6 in	2.50	0.009	
3	ECR	No. 5 @ 6 in	2.50	0.009	
4	ECR	No. 5 @ 6 in	2.50	0.009	
5	UNS S24100	No. 5 @ 6 in	2.50	0.009	
6	UNS S24100	No. 5 @ 6 in	2.50	0.009	
7	ASTM A1035	No. 5 @ 6 in	2.50	0.009	One-to-One Replacement
8	ASTM A1035	No. 5 @ 6 in	2.50	0.009	
9	UNS S32304	No. 5 @ 6 in	2.50	0.009	
10	UNS S32304	No. 5 @ 6 in	2.50	0.009	
11	GFRP	No. 5 @ 4 in	2.50	0.014	
12	GFRP	No. 5 @ 4 in	2.50	0.014	
13	ASTM A1035	No. 4 @ 7 in	2.50	0.0047	Reduced Bar Size
14	ASTM A1035	No. 4 @ 7 in	2.50	0.0047	
15	UNS S32304	No. 4 @ 5 in	2.50	0.0066	
16	UNS S32304	No. 4 @ 5 in	2.50	0.0066	
17	ASTM A1035	No. 4 @ 7 in	2.00	0.0044	Reduced Bar Size and Cover
18	ASTM A1035	No. 4 @ 7 in	2.00	0.0044	
19	UNS S32304	No. 4 @ 5 in	2.00	0.0061	
20	UNS S32304	No. 4 @ 5 in	2.00	0.0061	

Phase I

The CRR bar types included ASTM A1035, UNS S24100 stainless steel, UNS S32304 stainless steel and GFRP. The rebar size and spacing was kept the same throughout the first twelve specimens except for the two GFRP tests (T11 & T12) where the bar spacing was decreased from 6 to 4 in consistent with a typical GFRP bridge deck design. The additional GFRP quantity compensates for a 30% lower elastic modulus compared to steel which can result in wider crack widths if treated as a one-to-one replacement for steel.

CRR quantities were reduced by a bar size in the next four conducted tests (T13-T16), bar spacing was increased in the ASTM A1035 specimens (T13-T14) from 6 to 7 in, and decreased in the UNS S32304 reinforced slabs (T15-T16) from 6 to 5 in. These spacings and related reinforcement ratio, ρ as defined next in Eq. (1), were selected to produce a moment-curvature response consistent with that of the Grade 60 control. A last test set (T17-T20) was performed to study the influence of a reduction in concrete clear cover from 2.5 in to 2.0 in. The compression reinforcement layer was not embedded in the concrete specimens because VDOT

Table 2. Phase II Test Matrix

Test Number	Bar Type	Bar Quantity	Clear Cover (in)	Reinforcement Type	Reinforcement Ratio, ρ	Test Variable
1	Grade 60	No. 5 @ 6 in	2.50	Single reinf.	0.009	Second reinf. layer influence
2	Grade 60	No. 5 @ 6 in	2.50	Single reinf.	0.009	
3	Grade 60	No. 5 @ 6 in	2.50	Double reinf.	0.009	Controls
4	Grade 60	No. 5 @ 6 in	2.50	Double reinf.	0.009	
5	ASTM A1035	No. 4 @ 6 in	2.50	Double reinf.	0.0057	Reduced Bar Size
6	ASTM A1035	No. 4 @ 6 in	2.50	Double reinf.	0.0057	
7	UNS S32304	No. 4 @ 6 in	2.50	Double reinf.	0.0057	
8	UNS S32304	No. 4 @ 6 in	2.50	Double reinf.	0.0057	
9	ASTM A1035	No. 4 @ 6 in	2.00	Double reinf.	0.0052	Reduced Bar Size and Cover
10	ASTM A1035	No. 4 @ 6 in	2.00	Double reinf.	0.0052	
11	UNS S32304	No. 4 @ 6 in	2.00	Double reinf.	0.0052	
12	UNS S32304	No. 4 @ 6 in	2.00	Double reinf.	0.0052	
13	CFRP	No. 3 @ 6 in	2.00	Double reinf.	0.0029	Reduced Bar Size and Cover
14	CFRP	No. 3 @ 6 in	2.00	Double reinf.	0.0029	
15	BFRP	No. 5 @ 6 in	2.00	Double reinf.	0.0083	
16	BFRP	No. 5 @ 6 in	2.00	Double reinf.	0.0083	

does not consider this steel in a typical bridge deck design. The use of a single layer of tension reinforcement also provides a lower bound on serviceability and strength compared to an actual VDOT bridge deck design which employs a truss bar layout that varies the amount of compression steel in the deck (VDOT 2011). The reinforcement ratio is given for all the specimens in Tables 1 and 2.

$$\rho = A_s / bd \qquad \text{[Eq. 1]}$$

where

A_s is the steel reinforcement area in concrete beam design.
b is the cross-sectional width.
d is the effective depth from the top of the reinforced concrete beam to the centroid of the tensile steel.

Phase II

Grade 60 (uncoated), ASTM A1035, UNS S32304 stainless steel, BFRP and CFRP were included in this phase. The reinforcing bar sizes were reduced for all the ASTM A1035 and UNS S32304 specimens (T5-T12). Tests including a smaller clear cover (T9-T16), 2.0 in instead of 2.5 in, were conducted for all CRR bar types studied in this phase.

BFRP bar size and spacing were kept the same as that of a typical grade 60 bridge deck design (T15-T16) and CFRP bar sizes were reduced to No. 3 bars (T13-T14) because analytical model results from Response 2000 predicted a higher nominal moment strength than the control tests. The compression reinforcement was included in the specimens; nevertheless tests were also conducted without it to detect its effects on the flexural behavior.

Test Setup

All specimens were tested as simply-supported one-way beams-strips subjected to four-point bending. The center-to-center bearing spacing is 12 ft and the load points are at 4 ft and 8 ft from the roller bearing centerline (Figure 3). The flexural tests were conducted with the structural loading frame shown in Figure 3a. The frame provided a self-equilibrating reaction for a 220 kip MTS tension/compression servo-controlled hydraulic actuator.

The cross section B-B referenced in Figure 3(b) varies throughout the experimental program. The typical cross sections are shown in Figures 4 and 5 for Phase I and II, respectively.

For each slab specimen, two strain gages per reinforcement layer (e.g., bottom and top layers) were attached to the reinforcement at midspan to monitor strain during loading. Additionally, Bridge Diagnostic Inc. (BDI) strain transducers were attached directly to the concrete surface and to the sides along the constant moment region to measure the concrete compressive strains. These BDI transducers have an accuracy of ±20 με. Wire potentiometers with an accuracy of ±0.005 in were used to measure specimen deflection; potentiometers were placed at midspan, quarter-points as well as at the specimen supports to measure support settlement. The actuator's internal load cell was used to monitor applied load and a data acquisition system was used to record the experimental measures. Due to a flexural shear failure observed in some of the early specimens of the Phase I, external shear reinforcement was placed in the shear span for some of the specimens of the Phase I (Bowen, 2013) and "S" shaped Grade 60 bars were embedded in the concrete in the shear regions for the specimens of Phase II as shown in Figure 6.

Specimen Design

The concrete deck slabs were designed and detailed according to AASHTO LRFD Bridge Design Specifications (AASHTO 1996) and VDOT Modifications (VDOT 2010). The slabs were 168 in long, 36 in wide and 8.50 in thick.

Phase I

No. 4 bars were placed perpendicular to and on top of the specimen's longitudinal No. 5 bars (T1-T12) or No. 4 bars (T13-T20) at a 12 in spacing. Concrete clear cover to the longitudinal bars was kept constant to 2.5 in for the first sixteen tests and reduced to 2.0 in for the last four tests, and as mentioned previously, no top mat compression reinforcement was employed.

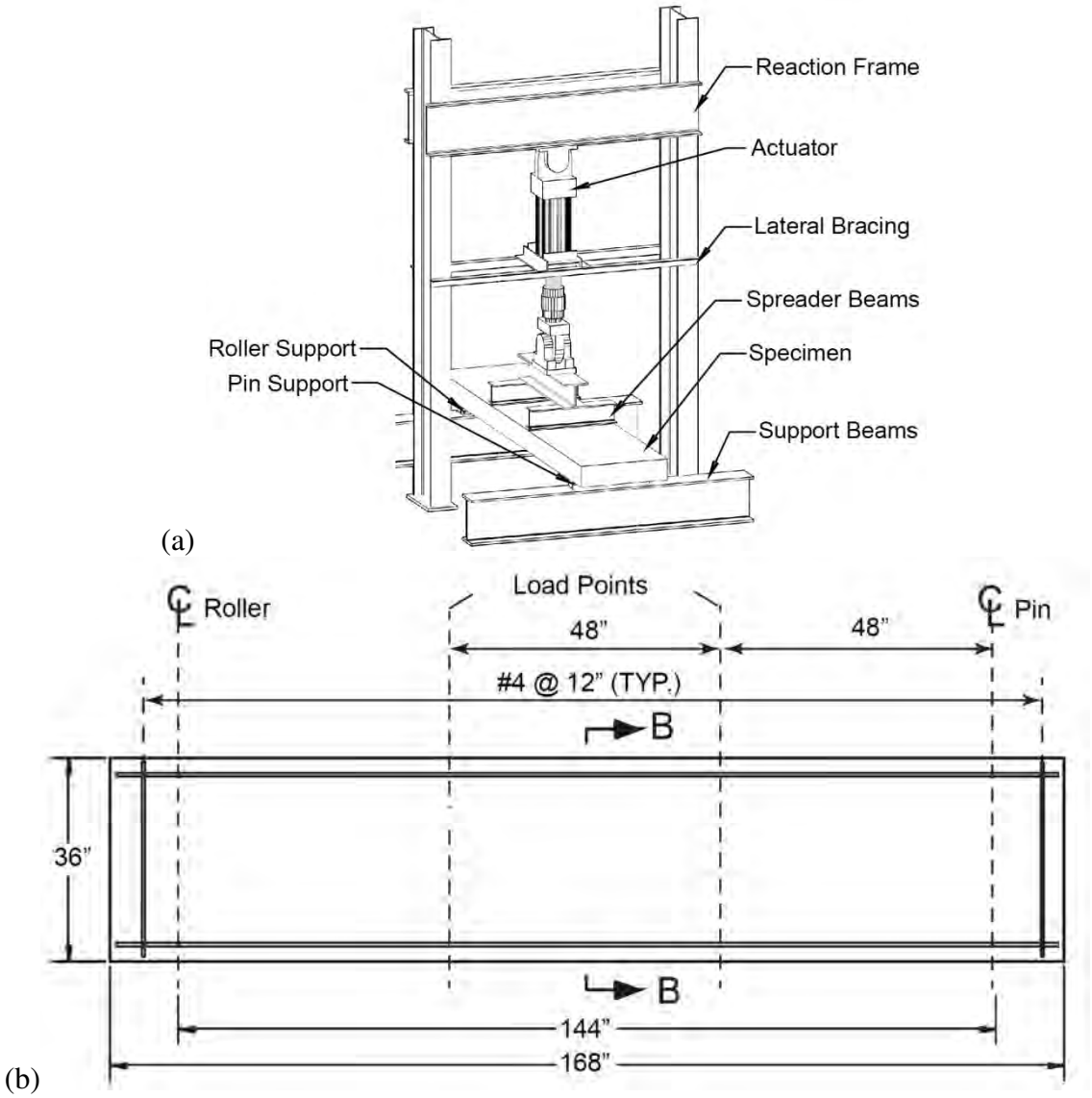

Figure 3. (a) Loading Frame. (b) Test Setup And Loading Points

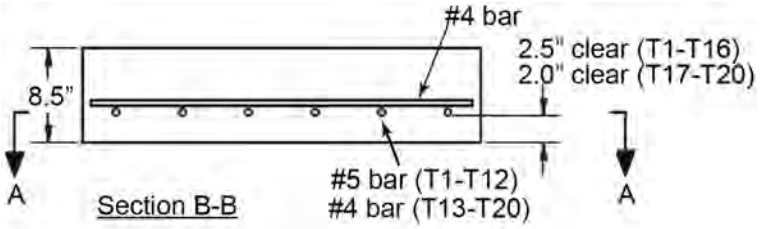

Figure 4. Typical Cross Sections for Phase I Specimens

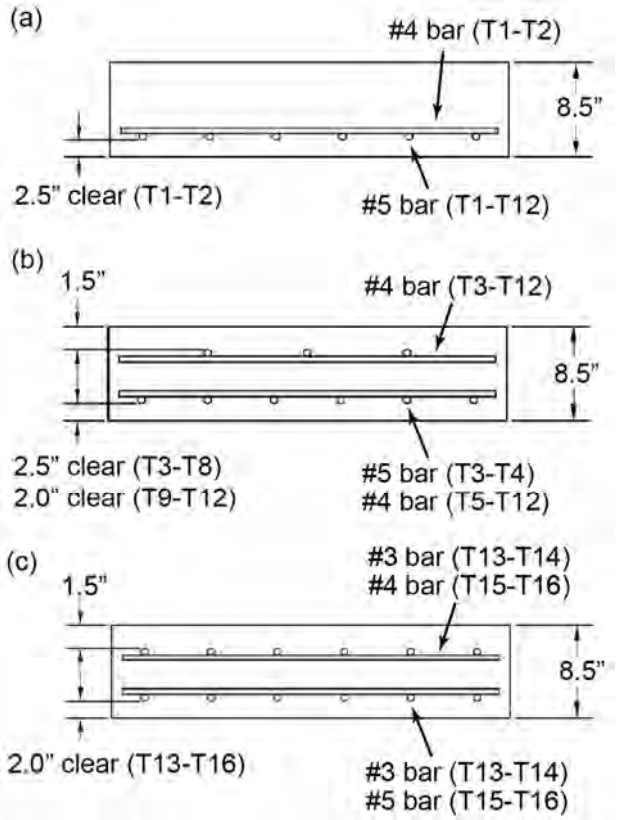

Figure 5. For Phase II Specimens in the B-B Section: (a) Cross Section T1-T2; (b) Cross Section T3-T12; (c) Cross Section T13-T16 (FRPs)

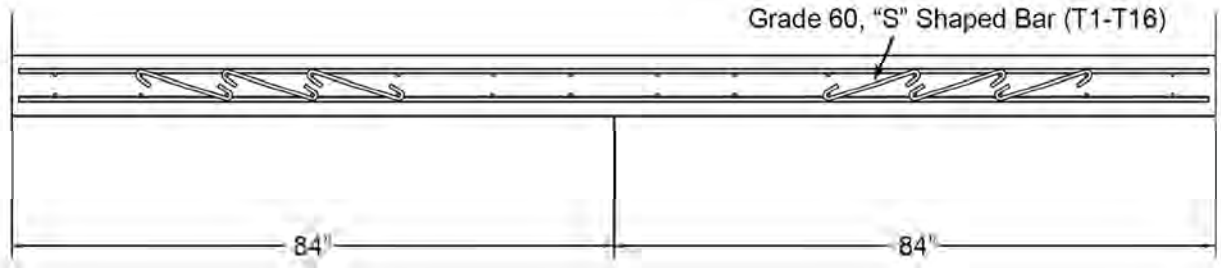

Figure 6. Shear Reinforcement for Specimens in Phase II

Phase II

No. 4 (T1-T12 & T15-T16) or No. 3 bars (T13-T14) were located perpendicular to the specimen's longitudinal bars (on top of the tension reinforcement and under the compression reinforcement) at a 12 in spacing. Concrete clear cover to the longitudinal bars remained constant to 2.5 in for the first eight tests and reduced to 2.0 in for the following eight tests.

Specimen Casting

Procedures

All specimens were cast with the VDOT general A4 superstructure concrete mix design commonly used in bridge decks (VDOT 2007). A minimum 28 day compressive strength of 4000 psi is provided by the A4 mix with No. 56 or 57 coarse aggregate, a maximum aggregate size of 1 in, and a water to cement ratio not greater than 0.45. The concrete was consolidated with electric spud vibrators, and hand trowels were used to finish the specimens. The slabs remained covered with plastic sheets for seven days. The formwork side faces were removed along with the plastic after this period.

As-Built Measurements

Slabs' clear cover was measured after rebar placement, and specimen width and depth dimension values were recorded prior to testing. Clear cover measurements were taken with a digital caliper along the constant moment region from the bottom of the form to the bottom of each placed bar at five different locations. Specimen depth and width were measured at ten and five locations on the slab, respectively.

The measured values differ slightly from the original specimen design of 36 in by 8.50 in and 2.50 in clear cover. A clear cover mean of 2.46 in and a coefficient of variation (COV) of 1.4% and 2.18% were calculated considering all the specimens in Phase I and II, respectively.

In Phase I, the means and COV for depth and width were calculated to be 8.71 in and 1.0%, and 36.40 in and 0.6%, respectively. For Phase II specimens, the means and COV for depth and width were calculated to be 8.91 in and 2.3%, and 36.14 in and 0.78%, correspondingly.

Material Properties

Rebar Properties

Relative rib area was measured as specified by the ACI 408R-03 report (ACI 2003). Tensile tests of all rebar specimens were conducted in accordance with ASTM A370 (ASTM 2005). Yield strength, ultimate strength, and the fracture strength of the rebar specimens, as well as the general stress-strain diagrams were obtained for each bar type in Phase I (Bowen, 2013) and Phase II (Salomon and Moen, 2014).

Yield strength for Grade 60 and ECR rebar was determined by identifying the stress where the first departure from linearity occurred. Since for all studied CRRs the stress-strain curve lacks a sharp yield plateau, yield strength was determined by the 0.2% offset method. Yield stress values corresponding to 0.0035 strain (0.35 EUL) were also defined and analyzed.

Concrete Properties

Freshly Mixed State

A series of tests were performed prior to the concrete placement in the specimen forms to check that the freshly mixed properties were consistent with the VDOT A4 concrete specification ranges. A cubic yard of the specimen concrete was on average composed of 1,780 lb of No. 57 coarse aggregate, 1,180 lb of fine sand aggregate, 535 lb of cement, 204 lb of water, and 135 lb of fly ash. A slump test was conducted in accordance with ASTM C143 (ASTM 2010b) to determine the concrete workability. Air content was measured according to ASTM C231 (ASTM 2010c). Further, concrete temperature was measured at the time of placement according to ASTM C1064 (ASTM 2008).

Hardened State

A group of 24 – 4 in × 8 in concrete cylinders were prepared at the time of concrete placement in general accordance with ASTM C192 (ASTM 2007) and were cured under ideal conditions in a moist-curing room (Phase I) or right next to the specimens under identical conditions (Phase II). The cylinder compressive strength was determined at 7, 14, 28, and 56 days from the placement date as the average of three tests. Additionally, three cylinders were tested at 28 days to obtain the concrete's tension splitting strength according to ASTM C496 (ASTM 2004).

Test Procedure

The slabs with simply-supported ends were subjected to a four point bending condition. The slab was loaded in displacement control at a rate of 0.15 in/min. This load rate was determined based on a strain rate diagram for steel (Moncarz et al., 1981), the intent being to avoid strain rate effects in the reinforcing bars. The specimens were loaded at 5 kip increments up to failure under static loading, and at each different loading stage, crack widths and crack propagation were measured with a crack microscope. Four cracks along a specimen's constant moment region– two on each side of the slab – were followed through the test in order to observe their increase in width and propagation patterns. Crack patterns were also captured with new computer vision techniques and a digital camera (Torok et al., 2012; Zheng and Moen, 2013) resulting in 3D point clouds of each specimen. At the end of the experiment, crack spacings were measured with digital calipers. A Vishay System 5000 data acquisition system recorded applied loads, deflections, and concrete and reinforcement strains.

Response 2000 Modeling Approach

Computational sectional analyses were performed with Response 2000. Response 2000 can perform different types of analysis, including flexural strain-compatibility calculations

including cracking that assume no shear or axial loads, and returns the moment-curvature relationship. For this research study, Response 2000's flexural analysis feature was used to determine the section moment-curvature containing each bar type.

Response 2000 uses a graphical interface to create a cross section. The program allows the user to define concrete strength, longitudinal bar strength, and transverse bar strength. These properties can be later modified in order to enter the material stress-strain curve. The interface also allows the user to input the bar size, spacing, and rebar number. Section geometry is defined by the user.

RESULTS AND DISCUSSION

Material Properties

Rebar Properties

Relative Rib Area

Tables 3 and 4 provide a statistical analysis overview of the relative rib areas for each bar type included in the experimental program. The variation in relative rib area between bar types is small, with the UNS S32304 stainless bar having the lowest at 0.068 in^2 in Phase I and 0.066 in^2 in Phase 2, which are about 20% below that of the Grade 60 at 0.086 in^2. The source of variation between bar types can be attributed to several factors, including manufacturing processes and measurement error. The variability in relative rib area within a specific bar type grouping was also minimal except the UNS S32304 stainless steel bars which had a COV of 10.9% in Phase I. This high relative rib area variability within the UNS S32304 bar group is attributed to the inconsistencies in the deformed bar patterns.

Table 3. Statistical Data for Relative Rib Area Within a Bar Type And Size (Phase I)

Rebar Specimen	Number Measured	Average Rib Area (in2)	COV (%)
Grade 60	4	0.086	1.3
ECR	4	0.085	2.2
UNS S24100	4	0.079	3.1
ASTM A1035	4	0.090	5.3
UNS S32304	4	0.068	10.9
GFRP	4	0.082	4.6

Table 4. Statistical Data for Relative Rib Area Within a Bar Type And Size (Phase II)

Rebar Specimen	Number Measured	Average Rib Area (in2)	COV (%)
Grade 60	8	0.081	4.4%
ASTM A1035	8	0.091	3.8%
UNS S32304	8	0.066	7.2%

Tables 5 and 6 display the statistical variation in relative rib area among all bar types included in Phase I and II with respect to bar size. The variation in the relative rib area between bar sizes is small, with the No. 4 bars having the lowest at 0.081 in^2 which is about 10% below that of the No. 5 bars at 0.089 in^2. The variability in relative rib area within a specific bar size is minimal for the No. 4 bars, but high for the No. 5 bars, for Phase I, which had a COV of 11.5%. These values exceed, again, the 0.048 in^2 and 0.043 in^2 minimum relative rib area ASTM 615 standards for No. 5 and No. 4 bars, respectively.

Table 5. Relative Rib Area Variation Among All Bar Types With Respect to Bar Size (Phase I)

Bar Size	Number Tested	Average Rib Area (in^2)	COV (%)
4	24	0.081	2.8
5	8	0.089	11.5

Table 6. Relative Rib Area Variation Among All Bar Types With Respect to Bar Size (Phase II)

Bar Size	Number Tested	Average Rib Area (in^2)	COV (%)
4	24	0.080	13.9
5	8	0.087	8.4

Tensile Tests

Figures 7 and 8 present the engineering stress-strain diagrams for each bar type for Phases I and II, respectively.

Yield stress values corresponding to 0.0035 strain (0.35 EUL) were consistent (1-3% higher) than those obtained by the 0.2% offset method.

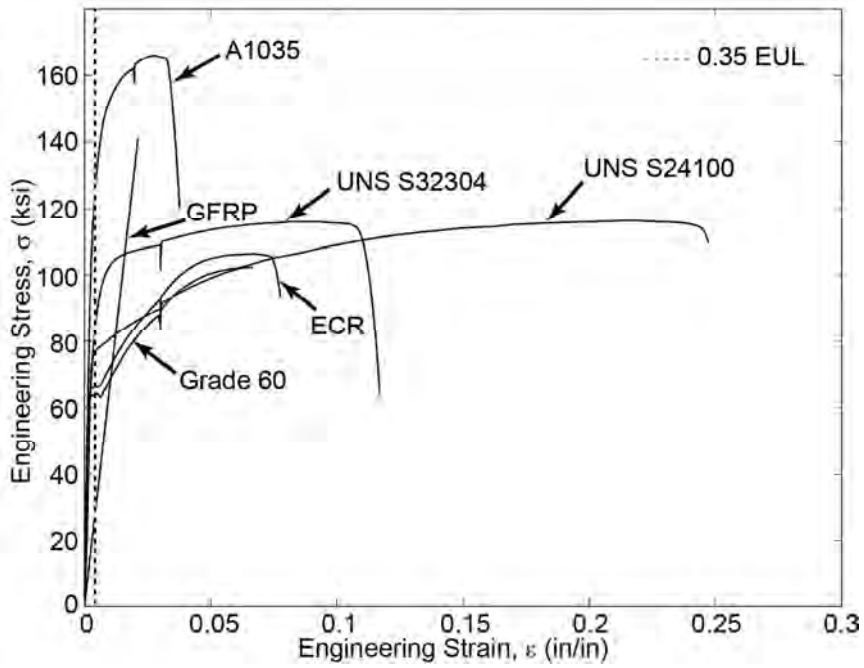

Figure 7. Stress-Strain Diagrams for Each Bar Type (Phase I)

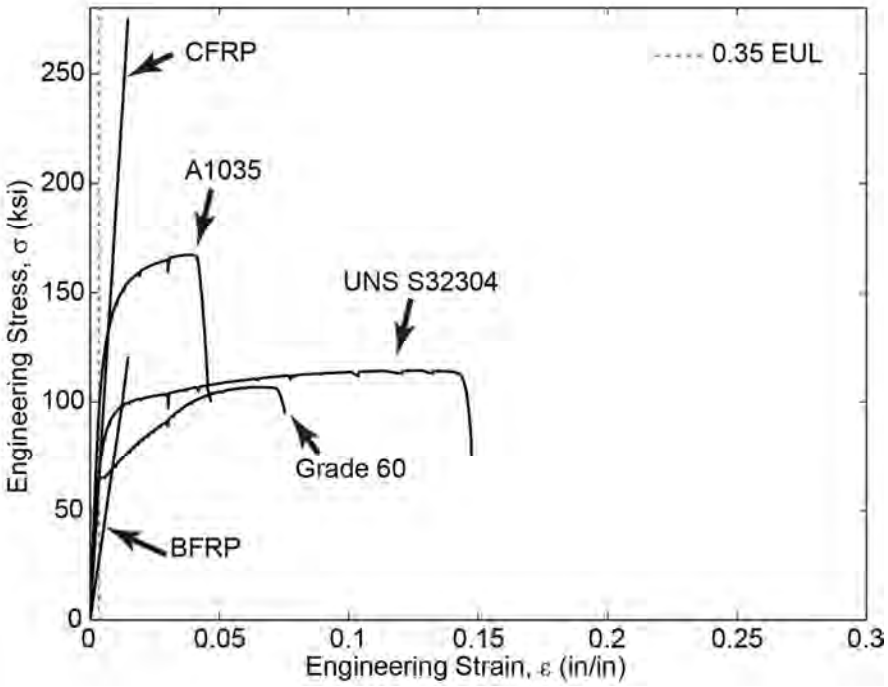

Figure 8. Stress-Strain Diagrams for Each Bar Type (Phase II). Note: BFRP Tensile Tests Did Not Reach the Ultimate Rebar Capacity Due to Slipping in the Test Setup

Concrete Properties

Freshly Mixed State

The actual measured concrete properties are provided in Tables 7 and 8 for Phases I and II, respectively.

Table 7. Phase I Specimens Concrete Properties in the Freshly Mixed State

Property	Test Number			
	T1-T6	T7-T12	T13-T16	T17-T20
Slump (in)	5.0	5.5	5.5	6.5
w/cm	0.34	0.45	0.45	0.50
Air (%)	6.00	4.75	5.00	6.50
Temperature (°F)	68	85	80	90

For the Phase I experimental program, the water to cement ratio (w/cm) for the first six specimens (T1-T6) is 25% lower than the w/cm for T7-T16 and 30% lower than the w/cm for T17-T20, and consequently, the measured slump was lower for T1-T6 than for the other tests as shown in Table 7. Air content in the concrete was measured to be between 4.75% and 6.5%. The difference in the concrete temperature at the time of placement is due to the weather temperature, even though all the slabs were cast inside the laboratory. While the first six specimens (T1-T6)

were cast in March 2012, the concrete placements for the next twelve slabs (T7-T16) were performed in late May and mid June 2012, and the last four slabs (T17-T20) were cast in early July 2012.

Table 8. Phase II Specimens Concrete Properties in the Freshly Mixed State

Property	Test Number			
	T1-T4	T5-T8	T9-T12	T12-T16
Slump (in)	7.5	7.5	5.5	6.5
w/c	0.39	0.40	0.37	0.36
Air (%)	6.60	7.00	5.50	8.00
Temperature (°F)	81	84	82	78

For the Phase II, the air content in the concrete was measured to be between 5.50% and 8.00%. There is almost no difference in the concrete temperature because all the specimens were cast inside the laboratory during the summer between June and August of 2013.

Hardened State

Tables 9 and 10 show the compressive and tensile strengths at 28 days obtained from the set of tests performed for Phases I and II, respectively. All tested values are available in (Bowen, 2013) and (Salomon and Moen, 2014).

Table 9. Concrete Properties in the Hardened State at 28 Days (Phase I)

Property	Test Number			
	T1-T6	T7-T12	T13-T16	T17-T20
Compressive strength (psi)	5110	4635	4500	4230
Tensile splitting strength (psi)	510	490	515	460

Table 10. Concrete Properties in the Hardened State at 28 Days (Phase II)

Property	Test Number			
	T1-T4	T5-T8	T9-T12	T12-T16
Compressive strength (psi)	3600	3130	4020	3570
Tensile splitting strength (psi)	450	380	430	470

Summary

Experimental results for the tested slabs are reported in Tables 11 and 12, including experimental ultimate moment, measured specimen yield strength, and crack width at the service moment, $M_{service}$=24.6 k-ft. The service moment is defined using the AASHTO LRFD Bridge Design Specifications (AASHTO 2010) and Chapter 10 in Part 2 of VDOT Manual of the Structure and Bridge Division (VDOT 2011) resulting in a dead (1.21 kip-ft/ft) plus live load (6.99 kip-ft/ft) moment of 8.2 kip-ft/ft × 3 ft = 24.6 kip-ft.

Phase I

Table 11. Test Results Summary (Phase I)

Test Number	Bar Type	Bar Quantity	Clear Cover (in)	Experimental Ultimate Moment M_{test} (kip-ft)	Measured Yield Strength f_y (ksi)	Crack Width @$M_{service}$ W_{cr} (in)
T1	Grade 60	No. 5 @ 6 in	2.50	65.0	63	0.006
T2	Grade 60	No. 5 @ 6 in	2.50	61.4	64	0.010
T3	ECR	No. 5 @ 6 in	2.50	64.8	66	0.013
T4	ECR	No. 5 @ 6 in	2.50	62.8	64	0.011
T5	UNS S24100	No. 5 @ 6 in	2.50	69.5	76	0.006
T6	UNS S24100	No. 5 @ 6 in	2.50	68.6	76	0.010
T7	ASTM A1035	No. 5 @ 6 in	2.50	105.0	120	0.011
T8	ASTM A1035	No. 5 @ 6 in	2.50	109.7	121	0.009
T9	UNS S32304	No. 5 @ 6 in	2.50	81.1	78	0.019*
T10	UNS S32304	No. 5 @ 6 in	2.50	82.6	80	0.014
T11	GFRP	No. 5 @ 4 in	2.50	80.4	138	0.025*
T12	GFRP	No. 5 @ 4 in	2.50	73.4	136	0.024*
T13	ASTM A1035	No. 4 @ 7 in	2.50	61.6	126	0.020*
T14	ASTM A1035	No. 4 @ 7 in	2.50	65.1	127	0.027*
T15	UNS S32304	No. 4 @ 5 in	2.50	58.3	90	0.018*
T16	UNS S32304	No. 4 @ 5 in	2.50	68.3	89	0.014
T17	ASTM A1035	No. 4 @ 7 in	2.00	75.4	130	0.015
T18	ASTM A1035	No. 4 @ 7 in	2.00	74.4	128	0.014
T19	UNS S32304	No. 4 @ 5 in	2.00	75.3	94	0.015
T20	UNS S32304	No. 4 @ 5 in	2.00	74.5	92	0.012

* W_{cr} values exceeding the AASHTO crack width limit of 0.017 in at service moment.

For a one-to-one rebar replacement, the flexural capacity, M_{test}, for the CRR specimens is always greater than the Grade 60 specimens. The highest flexural capacity was achieved with the ASTM A1035 specimens (T7 & T8), where M_{test} was approximately 70% larger than that of Grade 60 (T1, T2) resulting from the higher ASTM A1035 rebar yield stress. The GFRP specimens (T11, T12) had the largest crack widths, approximately 2.5 times wider than Grade 60 specimens at $M_{service}$.

The flexural capacity for the CRR specimens closely matches that of the Grade 60 specimens after a reduction of rebar size and increases by about 15% with a concrete clear cover reduction. While in the ASTM A1035 specimens a rebar reduction from No. 5 @ 6 in to No. 4 @ 7 in resulted in crack widths approximately 2.5 times wider at $M_{service}$ (T13, T14), crack widths in the UNS S32304 reinforced slabs (T15, T16) were unaffected by the decrease in bar size. This is due to the 30% higher reinforcement ratio, ρ, in the UNS S32304 specimens than

that in the ASTM A1035 reinforced slabs. Reducing clear cover decreased service crack widths by about 50% in the ASTM A1035 specimens (T17, T18) but, again, did not affect crack widths in the slabs reinforced with UNS S32304 steel (T19, T20).

Phase II

Table 12. Test Results Summary (Phase II)

Test Number	Bar Type	Bar Quantity	Clear Cover (in)	Experimental Ultimate Moment M_{test} (kip-ft)	Measured Yield Strength f_y (ksi)	Crack Width @$M_{service}$ W_{cr} (in)
T1	Grade 60	No. 5 @ 6 in	2.50	69.0	64	0.013
T2	Grade 60	No. 5 @ 6 in	2.50	67.0	65	0.012
T3	Grade 60	No. 5 @ 6 in	2.50	61.8	64	0.014
T4	Grade 60	No. 5 @ 6 in	2.50	73.6	65	0.011
T5	ASTM A1035	No. 4 @ 6 in	2.50	84.7	123	0.015
T6	ASTM A1035	No. 4 @ 6 in	2.50	88.0	125	0.014
T7	UNS S32304	No. 4 @ 6 in	2.50	60.4	84	0.027*
T8	UNS S32304	No. 4 @ 6 in	2.50	60.9	85	0.023*
T9	ASTM A1035	No. 4 @ 6 in	2.00	98.2	127	0.012
T10	ASTM A1035	No. 4 @ 6 in	2.00	93.6	125	0.012
T11	UNS S32304	No. 4 @ 6 in	2.00	68.6	80	0.015
T12	UNS S32304	No. 4 @ 6 in	2.00	65.0	84	0.015
T13	CFRP	No. 3 @ 6 in	2.00	87.4	280	0.041*
T14	CFRP	No. 3 @ 6 in	2.00	88.6	290	0.038*
T15	BFRP	No. 5 @ 6 in	2.00	95.8	118	0.039*
T16	BFRP	No. 5 @ 6 in	2.00	90.6	116	0.036*

* W_{cr} values exceeding the AASHTO crack width limit of 0.017 in at service moment.

The flexural capacity, $M_{test,}$ was always greater for the ASTM A1035 specimens (T5-T6 & T9-T10) than for the Grade 60 specimens (T3-T4), even though the bar size is one size smaller (0.2 in^2 instead of 0.31 in^2 of cross sectional area) which is equivalent to a reduction of 36% of steel. Decreasing the clear cover from 2.50 in to 2.00 in reduced the crack widths at $M_{service}$ 1.25 and 1.67 times for ASTM A1035 and UNS S32304 specimens, respectively.

Tests with UNS S32304 stainless steel (T7-T8 & T11-T12) presented similar flexural capacity than Grade 60 steel (T3-T4) and cracks widths 1.95 and 1.17 times wider for 2.50 in and 2.00 in clear cover, correspondingly. The M_{test} values were around 1.33 times higher for the BFRP and CFRP tests than for Grade 60. The FRP tests (CFRP and BFRP) resulted in crack widths 3 times wider than Grade 60 at $M_{service}$.

Moment-Curvature

In this research program, the curvature measurements were calculated using the measured concrete strain on the slab top surface and the measured rebar strain with the Euler-Bernoulli relationship as defined next in equation 2. The curvature measurements in the following figures do not go up to ultimate load because the BDI strain gages on the concrete were not able to obtain measurements up to ultimate load. Even though the moment-curvature plots are not complete, they show how each slab behaves prior to cracking, after cracking, during rebar yield, and after rebar yield. The slope of each line represents the flexural rigidity (EI) of the slab. The discontinuities in the load-displacement curves every 10 kip-ft are due to the load being stopped to measure crack widths.

Euler-Bernoulli relationship:

$$1/\rho = \varepsilon/y \qquad \text{[Eq. 2]}$$

where

ρ = radius of curvature
ε = engineering strain at location y from the neutral axis

Phase I

Figure 9 compares the measured moment-curvature relationships from the controls and one-to-one replacement experiments for each specimen type. The initial slope represents the beam stiffness prior to cracking which is consistent for each slab specimen type. The slopes begin to vary once the slabs crack, which occurs between 7 and 15 kip-ft (28% to 60% of $M_{service}$) for all the slabs. After cracking the slabs reinforced with ASTM A1035, Grade 60, ECR, and UNS S24100 all have similar flexural stiffness up to yield due to the similar rebar elastic modulus. The slabs reinforced with UNS S32304 and GFRP have a lower flexural stiffness after cracking because of their smaller rebar elastic modulus (approximately E=27000 ksi for the UNS S32304 stainless steel rebar and E=7000 ksi for GFRP).

The slabs reinforced with ECR and Grade 60 experience a plateau after yielding, where the slab loses most of its stiffness, followed by a slight increase in stiffness after the slab has experienced a large increase in curvature. This is due to the yield plateau and the strain hardening in the ECR and Grade 60 steel. The slabs reinforced with UNS S24100, UNS S32304, and ASTM A1035 experience a gradual loss in stiffness because of the rebar material properties, i.e., gradual yielding behavior. The slabs reinforced with GFRP experience the same stiffness throughout the test because of the material's linear elasticity up to failure.

Figures 10 and 11 show the influence of a reduction in rebar size and decrease in concrete clear cover on the ASTM A1035 (Figure 10) and UNS S32304 (Figure 11) specimen load-deformation response. The moment-curvature prior to cracking of the ASTM A1035 and UNS

S32304 slabs with reduced bar size and decreased cover is consistent with the Grade 60 reinforced slab and to that of the ASTM A1035 and UNS S32304 one-to-one replacement specimens. For the one-to-one ASTM A1035 and UNS S32304 replacement specimens (T7-T10), the slopes begin to vary once the slabs crack, which occur again between 7 and 15 kip-ft (28% to 60% of $M_{service}$). For the ASTM A1035 reinforced slabs, a decrease in the bar size results in a loss in flexural rigidity (45% increase in beam curvature at $M_{service}$) whereas a decrease in clear cover results in a gain in flexural rigidity (approximately 30% decrease in beam curvature at $M_{service}$). These results support a multi-tiered design approach to CRR, where reinforcement bar size, spacing and cover can be reduced together to meet or improve upon the structural performance of a typical Grade 60 bridge deck.

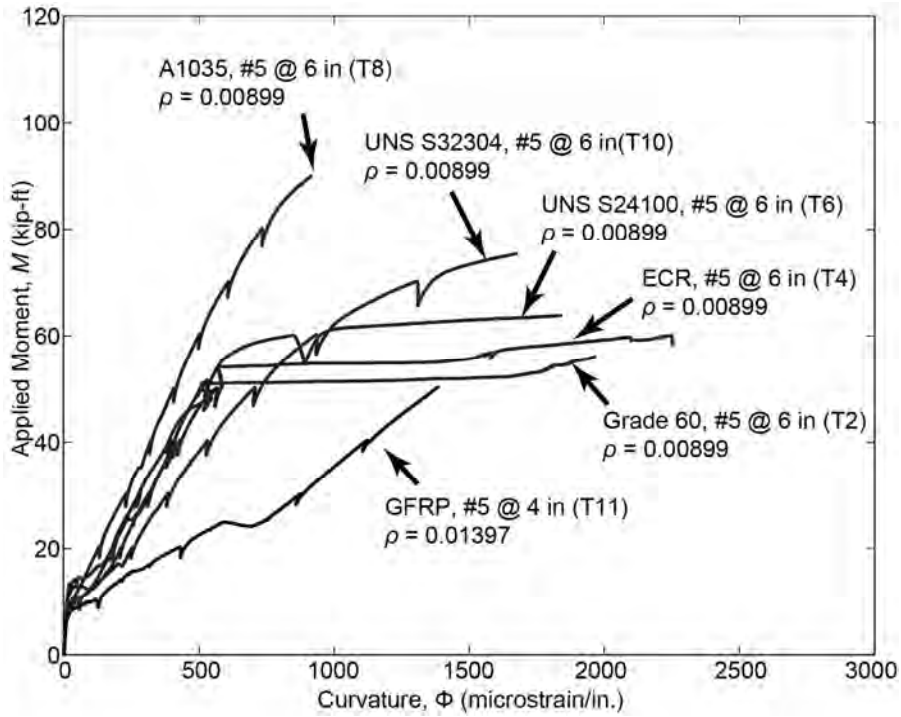

Figure 9. Moment-Curvature for Controls and One-To-One Replacement Experiments (Full Curve to Failure Is Not Shown Because the External Strain Gages Were Removed Before Failure)

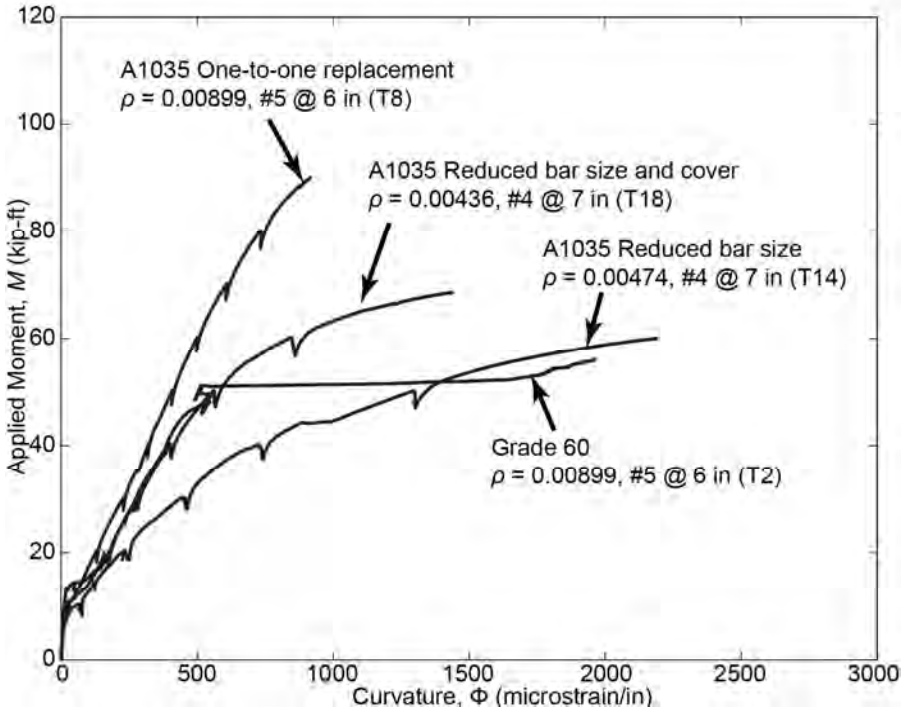

Figure 10. Moment-Curvature Comparison for the ASTM A1035 Reduced Bar Size and Cover Experiments to the Grade 60 Control

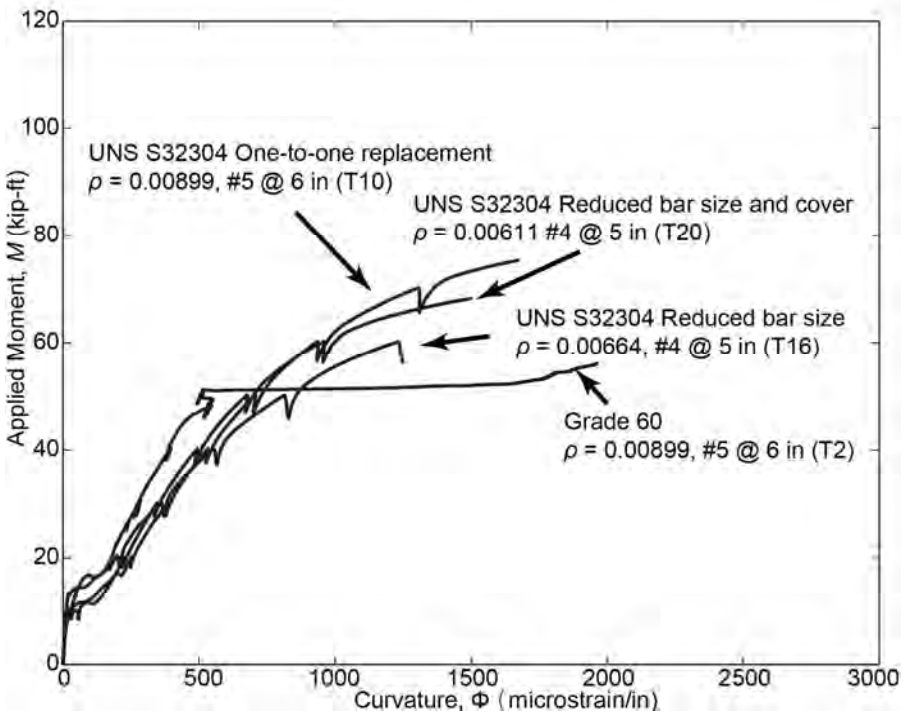

Figure 11. Moment-Curvature Comparison for the UNS S32304 Reduced Bar Size and Cover Experiments to the Grade 60 Control

Phase II

Figures 12 through 14 show the influence of a reduction in rebar diameter and a decrease in concrete cover on the ASTM A1035 (Figure 12), UNS S32304 (Figure 13), BFRP and CFRP (Figure 14) specimens on the load-deformation response. The moment-curvature prior to cracking of the ASTM A1035, UNS S32304 and FRP slabs with reduced bar size and decreased cover is consistent with the Grade 60 reinforced slab. The specimens with BFRP and CFRP cracked at a lower applied moment than Grade 60.

The specimens using No. 4 ASTM A1035 bars presented a slightly lower flexural stiffness than those reinforced with No. 5 Grade 60 bars. However, by decreasing the clear cover 0.5 in the ASTM A1035 specimens presented an almost identical flexural rigidity than the Grade 60 specimens. For the slabs reinforced with No.4 UNS S32304 bars, the flexural stiffness was lower than the Grade 60 and gradually decreased after cracking. Also, it is shown again how the flexural rigidity is increased by decreasing the clear cover. For all the FRP specimens the flexural rigidity was lower than the Grade 60 specimens because of the smaller rebar elastic modulus (approximately E = 8000 ksi for No. 5 BFRP rebar and E=18500 ksi for No. 3 CFRP) and because of the reduced bar size (No. 3 bars were used for the CFRP specimens instead of No. 5) for the CFRP. The FRP tests presented a linear behavior after cracking and throughout the testing due to the material's linear elasticity up to failure.

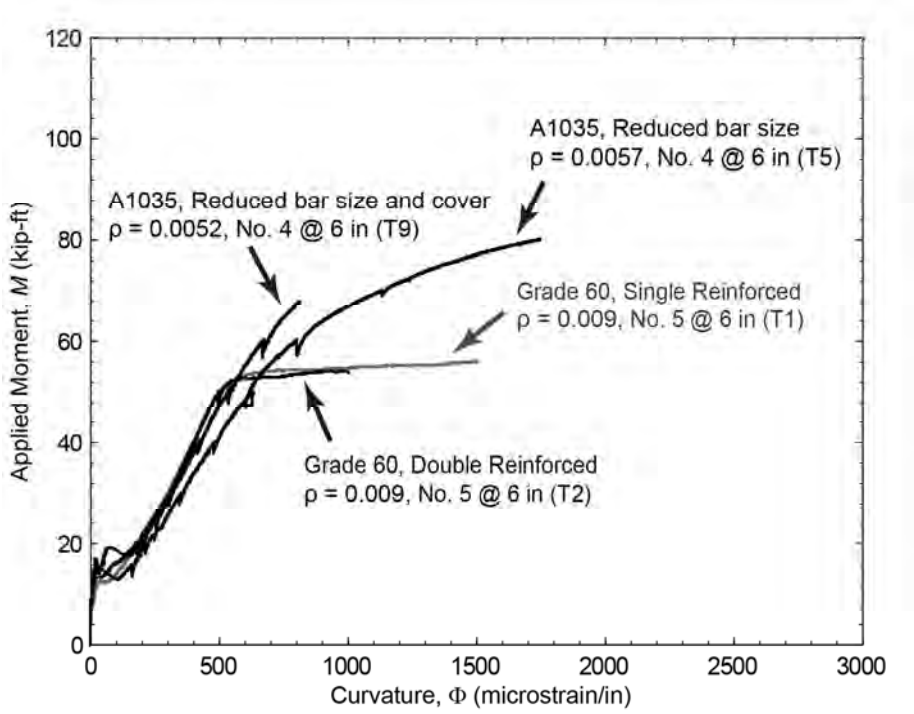

Figure 12. Moment-Curvature Comparison for the ASTM A1035 Experiments to the Grade 60 Controls (Full Curve to Failure Is Not Shown Because the External Strain Gages Were Removed Before Failure)

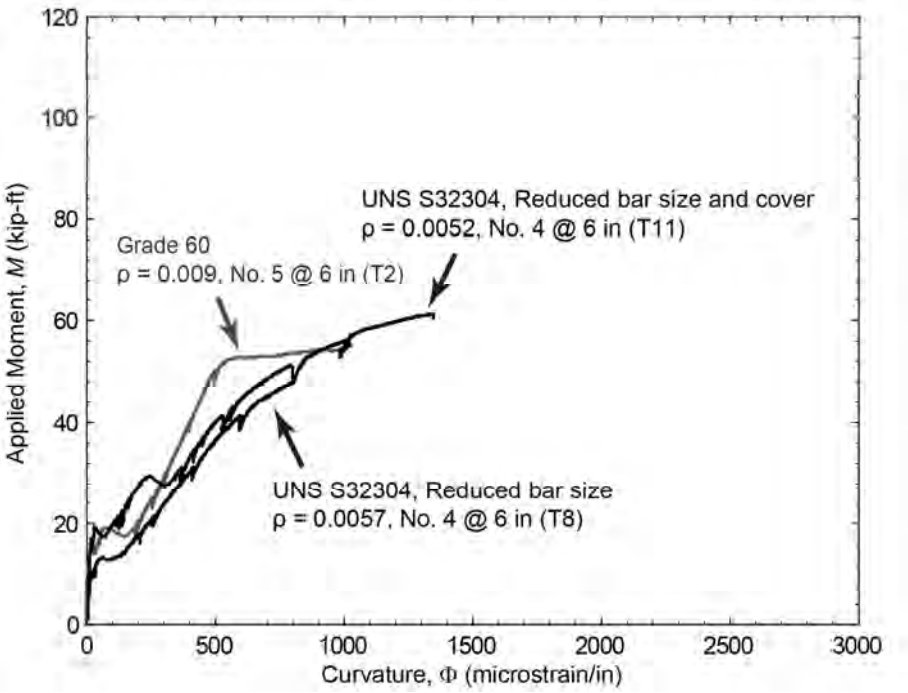

Figure 13. Moment-Curvature Comparison for the UNS S32304 Experiments to the Grade 60 Controls (Full Curve to Failure Is Not Shown Because the External Strain Gages Were Removed Before Failure)

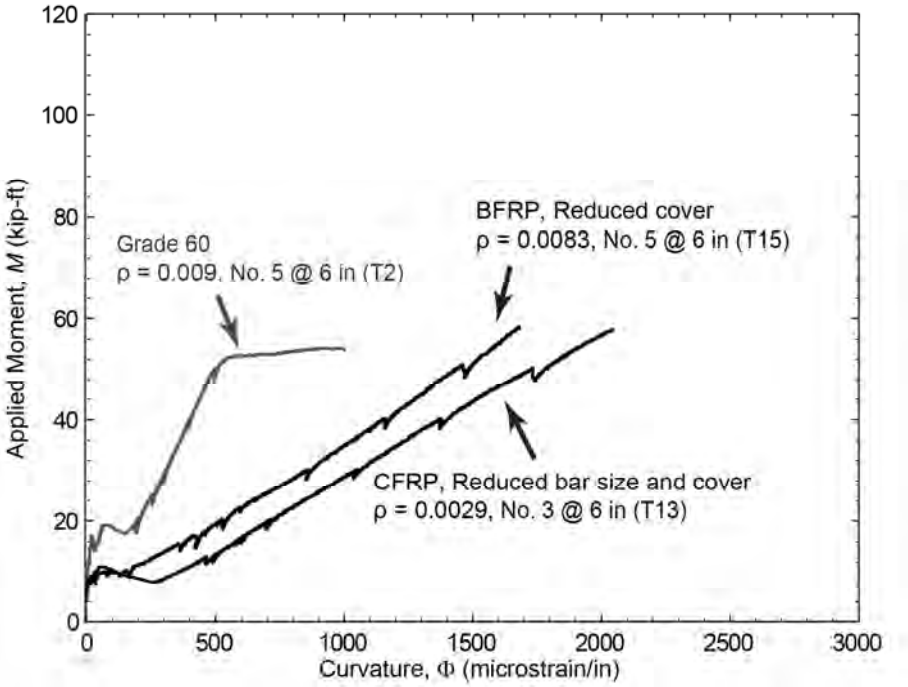

Figure 14. Moment-Curvature Comparison for the FRP Experiments to the Grade 60 Controls (Full Curve to Failure Is Not Shown Because the External Strain Gages Were Removed Before Failure)

Moment-Deflection Response

Phase I

Figures 15 through 17 show the influence of a reduction in rebar size and decrease in concrete clear cover on the ASTM A1035 (Figure 15), UNS S32304 (Figure 16), UNS S24100 and ECR (Figure 17) specimens in the moment-deflection response. The moment-deflection relationship prior to cracking of all the specimens was consistent with the Grade 60. Also, the deflection at the flexural capacity, M_{test}, increases as the slab flexural stiffness decreases.

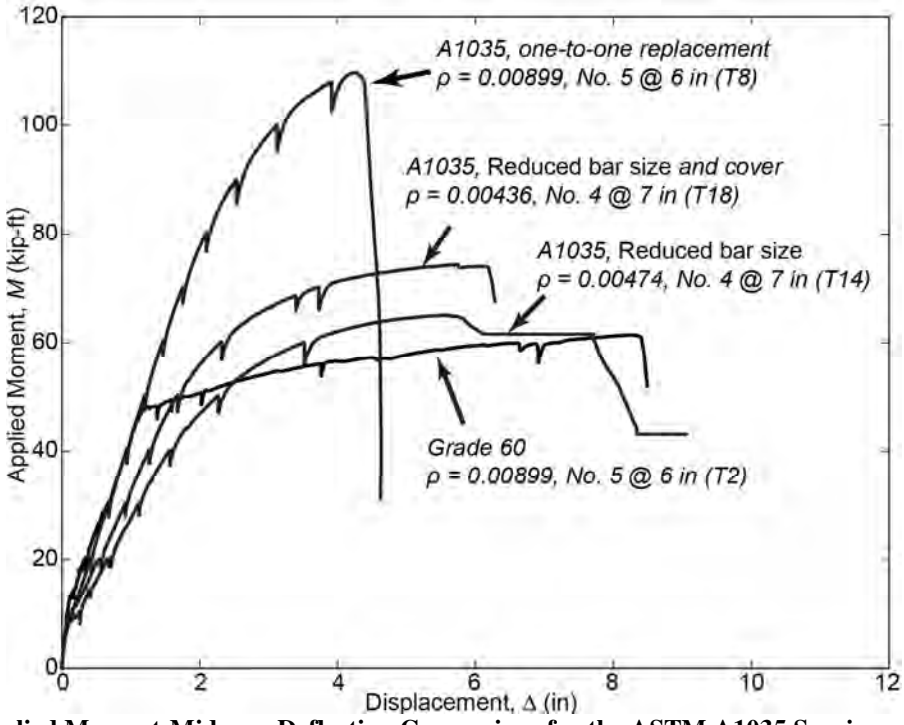

Figure 15. Applied Moment-Midspan Deflection Comparison for the ASTM A1035 Specimens to the Grade 60 Controls

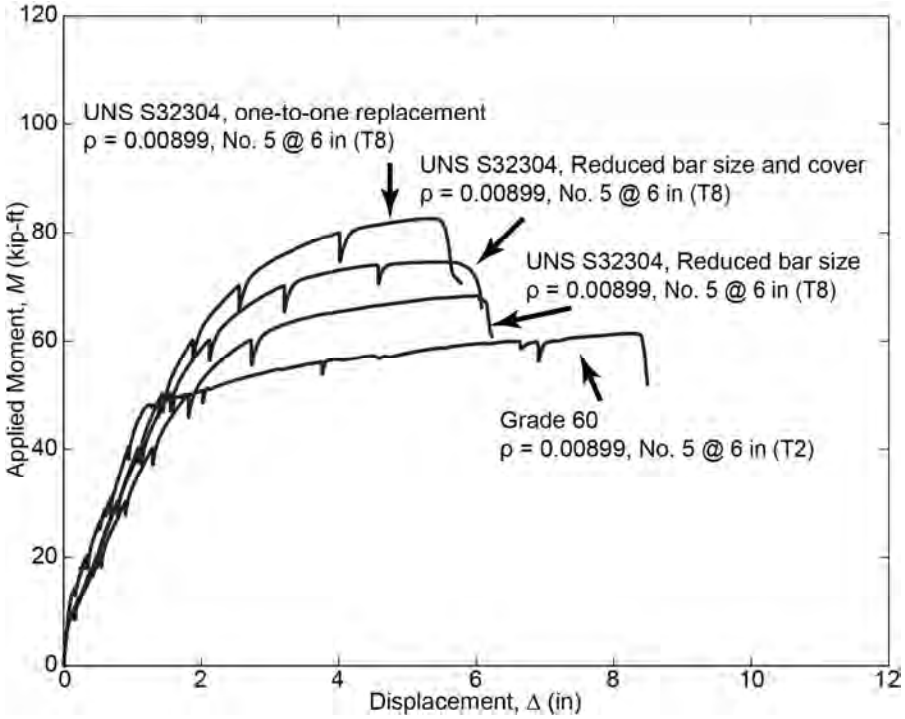

Figure 16. Applied Moment-Midspan Deflection Comparison for the UNS S32304 Specimens to the Grade 60 Controls

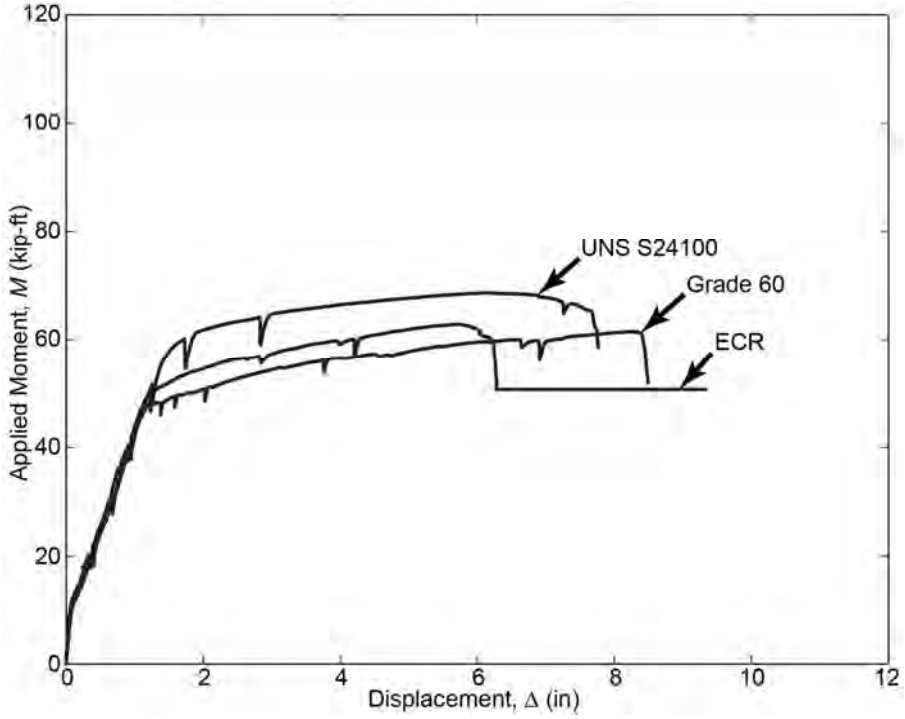

Figure 17. Applied Moment-Midspan Deflection Comparison for the UNS S24100 and ECR Specimens to the Grade 60 Controls

Phase II

Figure 18 illustrates the compression reinforcement influence in the specimen moment-deflection relationships. The strain gages attached to this layer of reinforcement are in compression until reaching the cracking moment, and then the rebar strains move from compression to tension. The compression reinforcement increases the strength of the concrete slab because it becomes extra tension reinforcement as the neutral axis rises in the slab. The compression reinforcement also reduces the deflection at the ultimate moment by 13% as shown in Figure 18.

A reduction in rebar diameter and a decrease in concrete cover on the ASTM A1035 (Figure 19) and UNS S32304 (Figure 20) produced a similar behavior to the Grade 60 specimens and a higher nominal flexural capacity for the ASTM A1035. Although the specimens using FRP showed a more flexible and linear behavior than those reinforced with Grade 60 (Figure 21), they reached a flexural strength 1.3 and 1.4 times higher than Grade 60 steel for CFRP and BFRP, respectively.

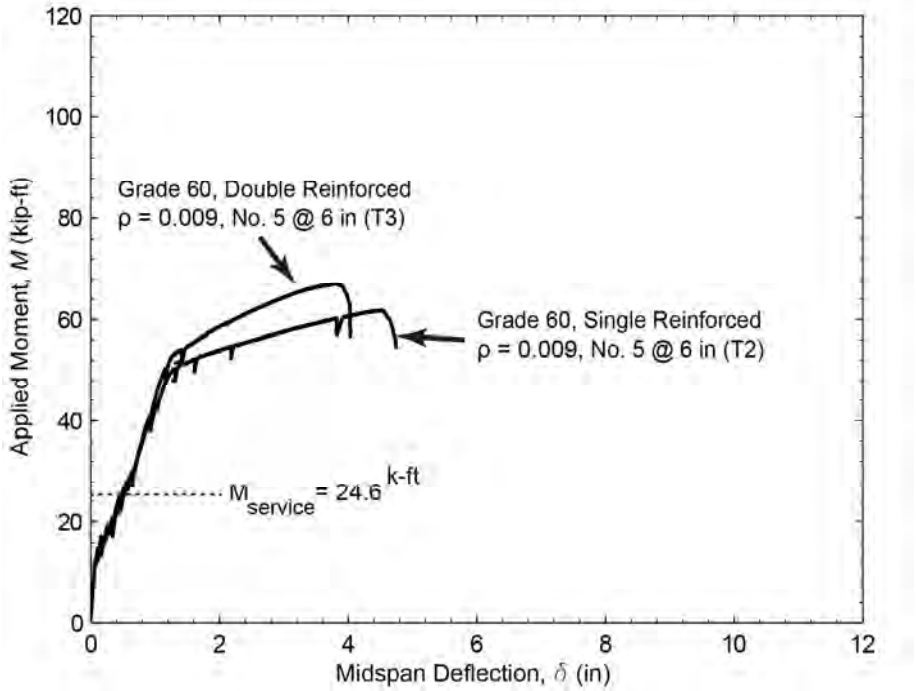

Figure 18. Applied Moment-Midspan Deflection Comparison Between the Double Layer Reinforced and the Single Layer Reinforced Specimens With Grade 60 Steel (Same Bar Size, Rebar Spacing and Specimen Dimensions)

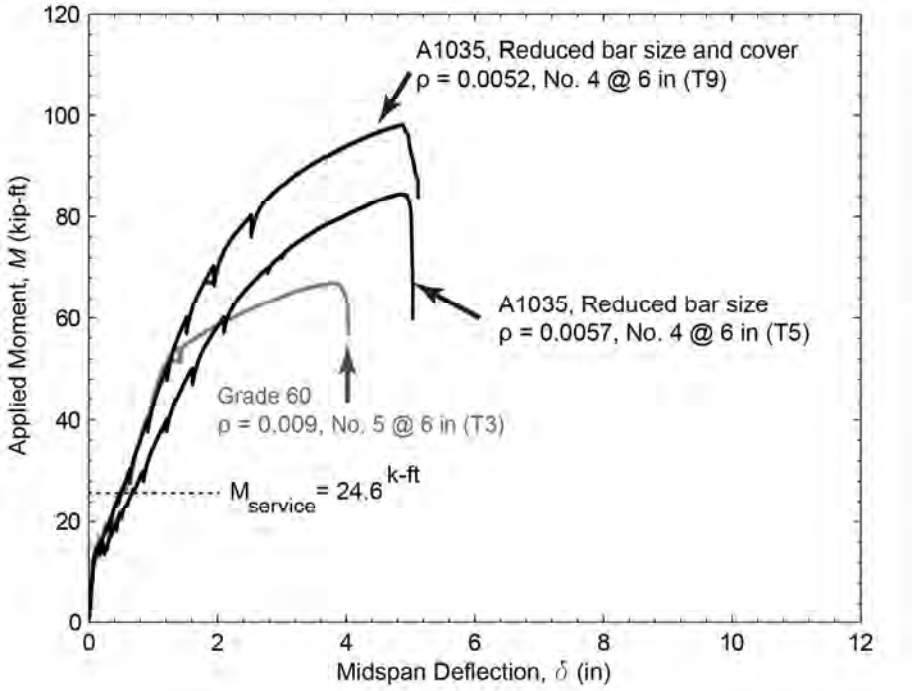

Figure 19. Applied Moment-Midspan Deflection Comparison for the ASTM A1035 Experiments to the Grade 60 Controls

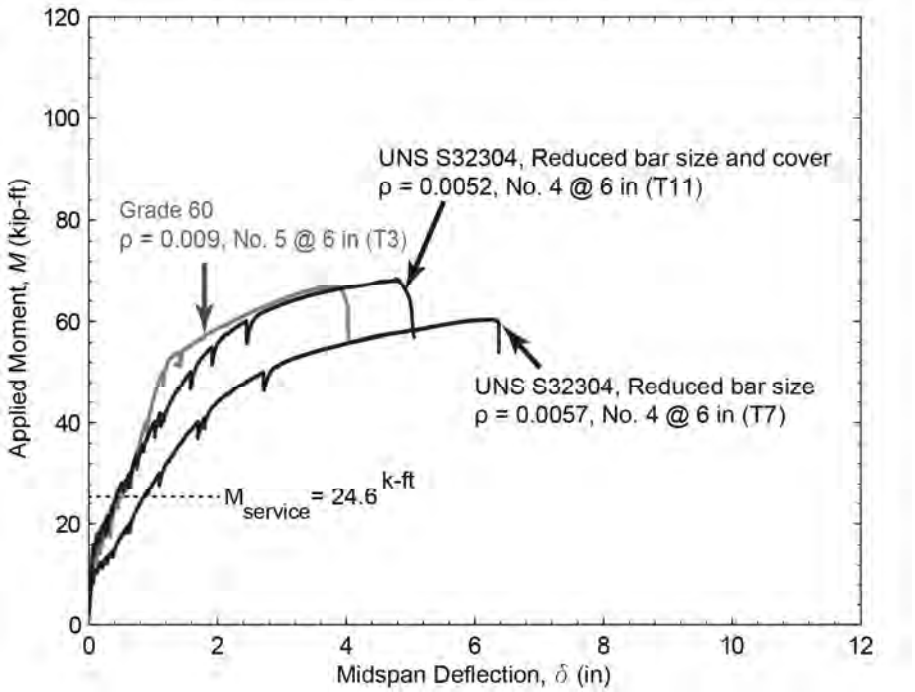

Figure 20. Applied Moment-Midspan Deflection Comparison for the UNS S32304 Experiments to the Grade 60 Controls

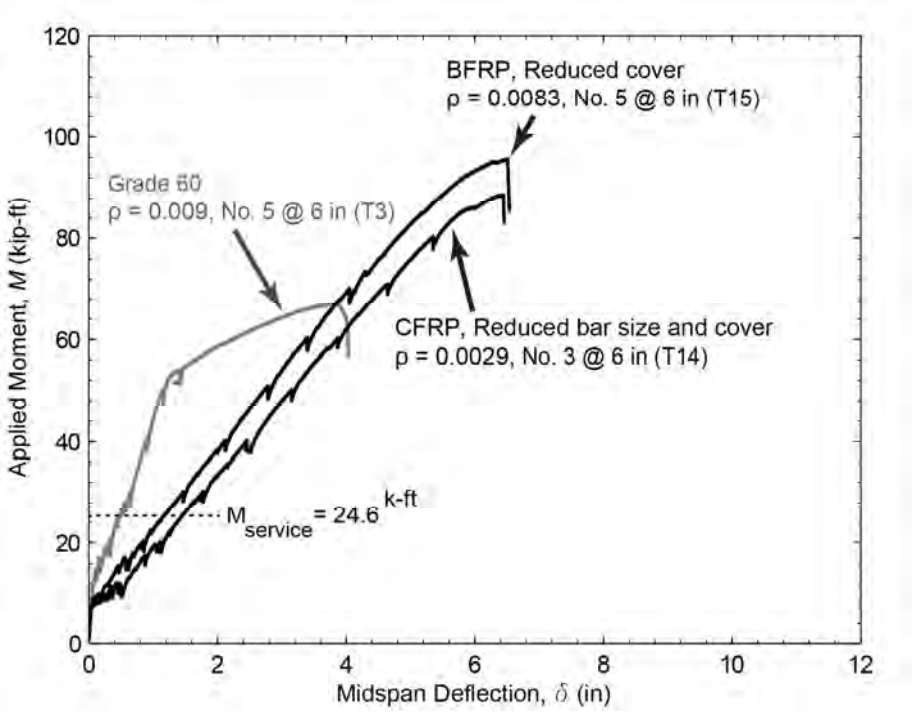

Figure 21. Applied Moment-Midspan Deflection Comparison for the FRP Experiments to the Grade 60 Controls

Concrete Crack Widths

Phase I

Figure 22 shows a comparison of the measured crack width in the controls and one-to-one replacement reinforced concrete slabs at different load levels. For all specimens, the first crack was initiated at a region near mid-span and as the load increased, additional cracks started to form throughout the specimen length, widening and propagating upward until failure occurred by concrete crushing. Crack widths are about 2.5, 3.3 and 3.2 times wider for the GFRP, BFRP and CFRP reinforced concrete slabs than for the steel reinforced specimens at $M_{service}$. This is mainly because of FRP rebar stiffnesses which are 70%, 70%, and 40% lower for GFRP, BFRP, and CFRP compared to that of the steel.

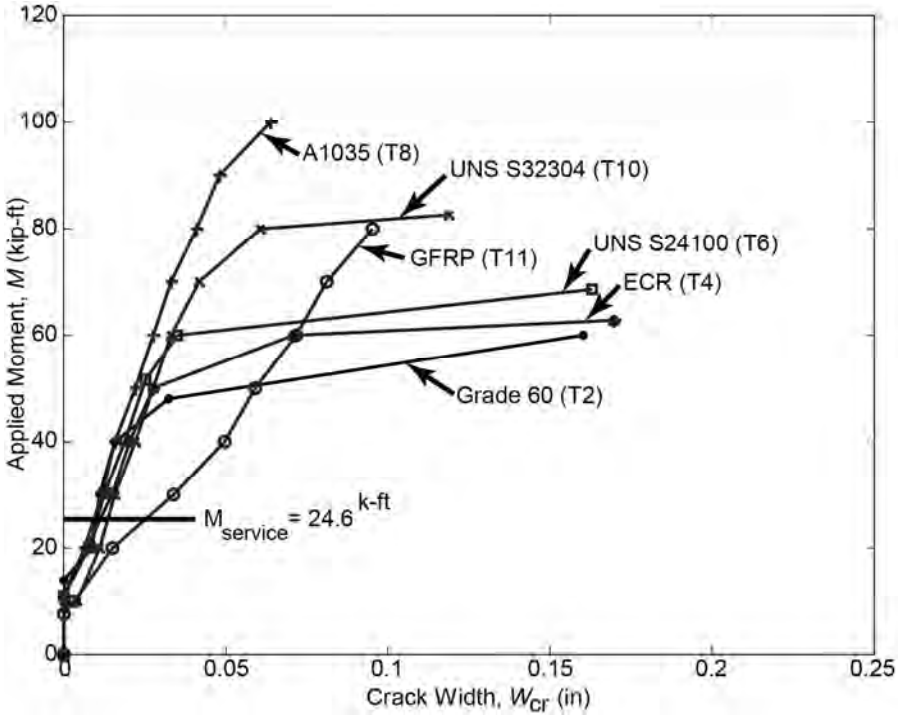

Figure 22. Comparison of Measured Crack Widths for Controls (No. 5 @ 6 In, ρ=0.009) and One-To-One Replacement (No. 5 @ 6 In, ρ=0.009 (T8, T10); No. 5 @ 4 In, ρ=0.014 (T11)) Experiments

Figures 23 and 24 illustrate the influence of a reduction of ASTM A1035 (Figure 23) and UNS S32304 (Figure 24) rebar size and the effects of a decrease in concrete clear cover on crack widths forming in the specimens reinforced with these bar types. As for previous tested specimens, the first crack was initiated at a region near mid-span and succeeding cracks propagated in the same manner until slab failure. For the ASTM A1035 specimens, crack widths are about 2.5 times wider at $M_{service}$ after rebar quantity reduction (ρ=0.009 to ρ=0.0047) and corresponding increase in spacing from 6 to 7 in, however the crack spacing reduced by 50% when clear cover was reduced (ρ=0.0047 to ρ=0.0044). For the slabs reinforced with UNS S32304, crack widths are consistent under the same load level after a rebar size reduction (ρ=0.009 to ρ=0.0066) and after a clear cover decrease (ρ=0.0066 to ρ=0.0061). Figures 23 and 24 indicate that crack widths are consistent for Grade 60 control and specimens reinforced with both ASTM A1035 (No. 4 @ 7 in) and UNS S32304 (No. 4 @ 5 in) bar types after a decrease in clear cover from 2.5 to 2.0 in.

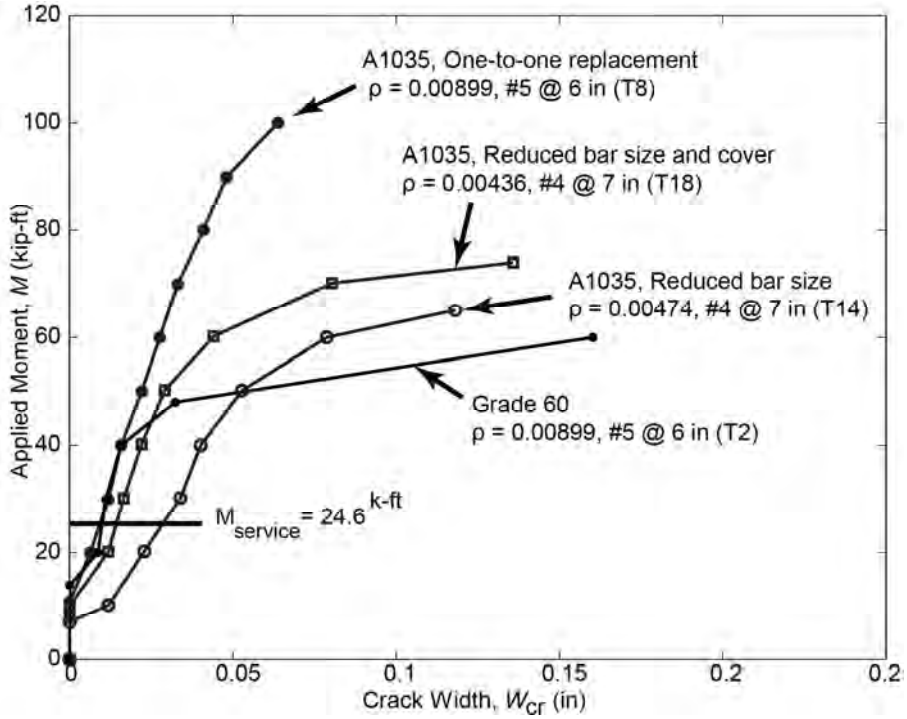

Figure 23. Comparison of Measured Crack Widths for the ASTM A1035 Reduced Bar Size and Cover Experiments to Grade 60 Control

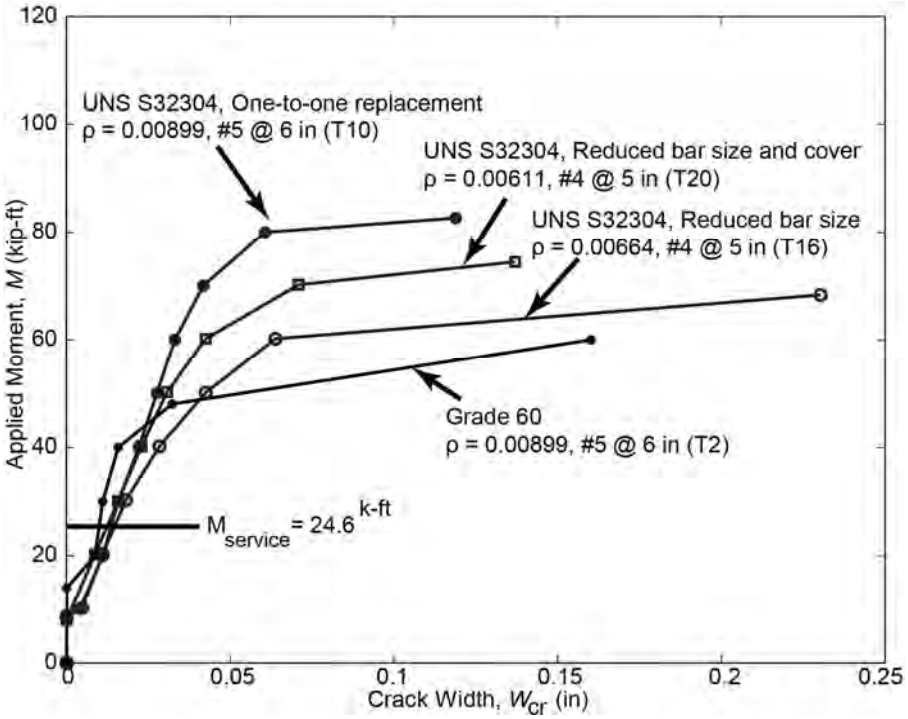

Figure 24. Comparison of Measured Crack Widths for the UNS S32304 Reduced Bar Size and Cover Experiments to Grade 60 Control

Phase II

Figure 25 illustrates the compression reinforcement influence on measured crack width, which is negligible below the proportional limit. For the ASTM A1035 (Figure 26) and UNS S32304 (Figure 27) tests, a reduction in rebar diameter and a decrease in concrete cover proved to be enough to comply with the AASHTO requirements for crack widths. For all specimens, the first crack was initiated at a region near mid-span and as the load increased, additional cracks started to form throughout the specimen length, widening and propagating upward until failure occurred by concrete crushing. For the BFRP and CFRP reinforced concrete slabs, crack widths were approximately 3 times wider than for the Grade 60 steel reinforced specimens at $M_{service}$ (Figure 28). This is due to the lower stiffness of the FRPs reinforcement compared to steel.

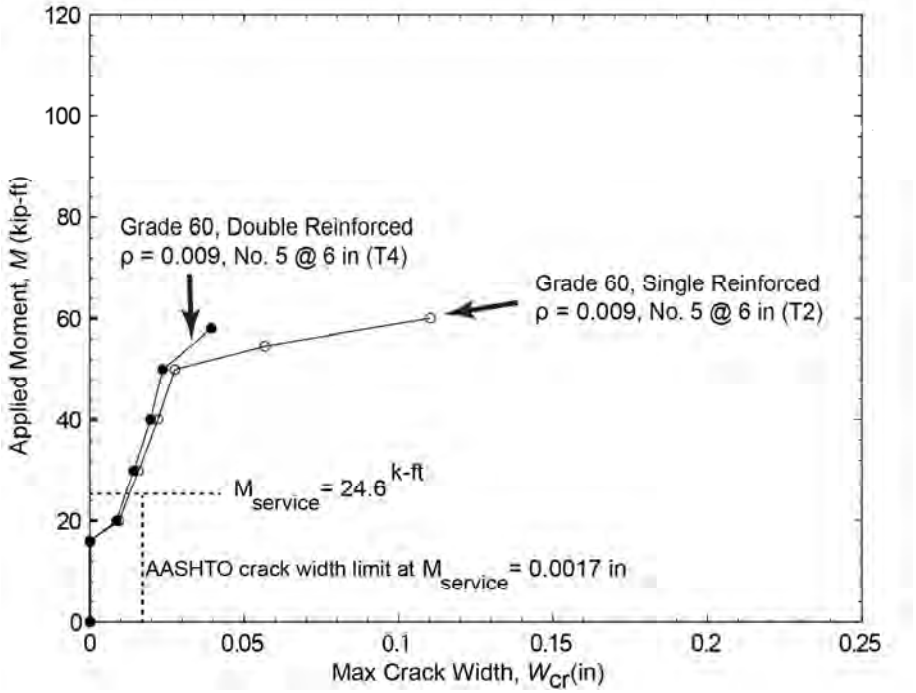

Figure 25. Applied Moment-Max Crack Width Comparison Between the Double Reinforced and the Single Reinforced Specimens With Grade 60 Steel

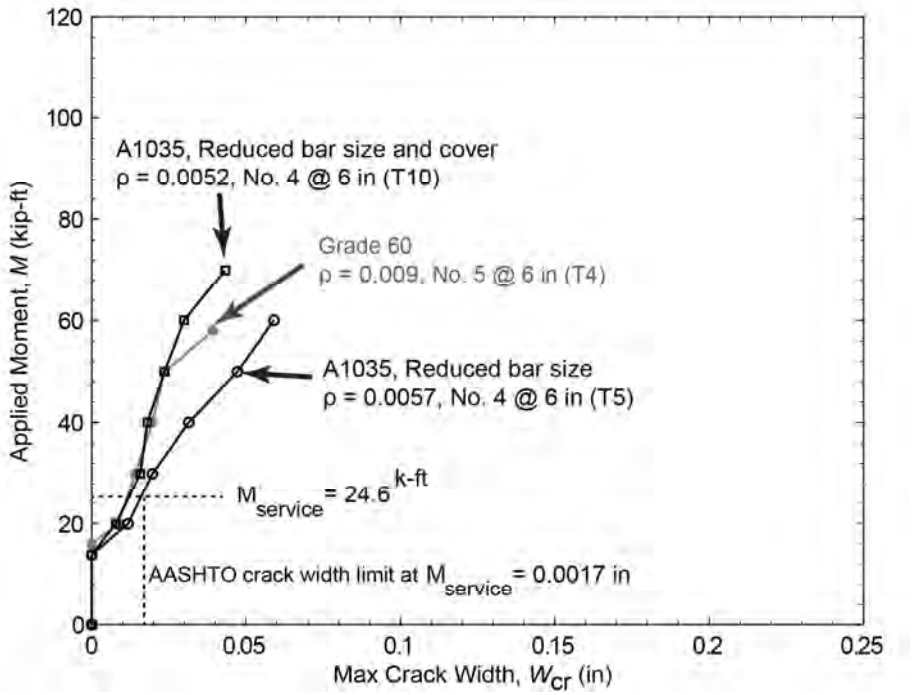

Figure 26. Applied Moment-Max Crack Width Comparison for the ASTM A1035 Experiments to the Grade 60 Controls

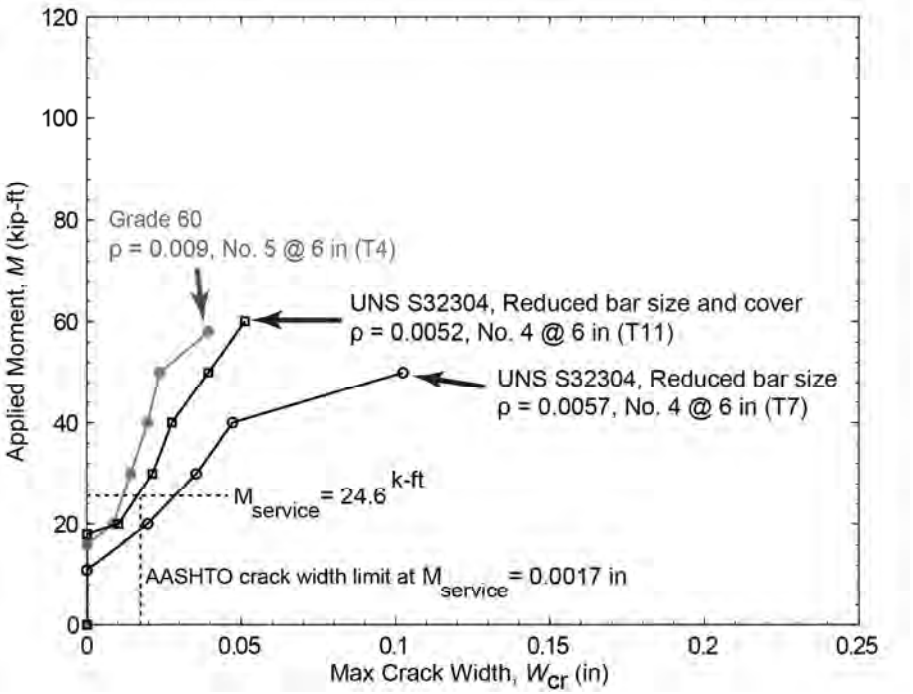

Figure 27. Applied Moment-Max Crack Width Comparison for the UNS S32304 Experiments to the Grade 60 Controls

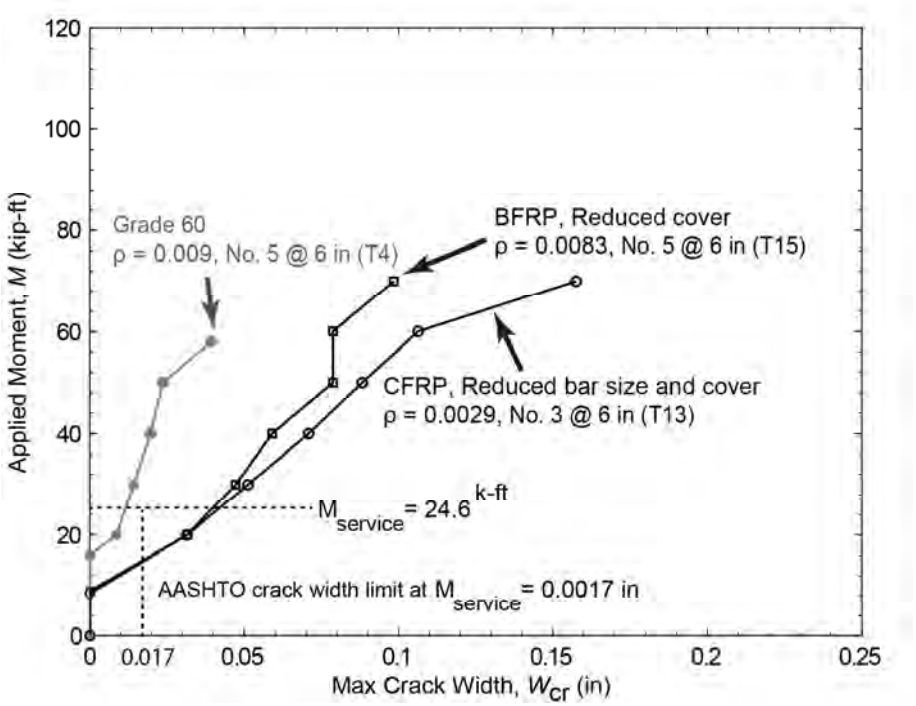

Figure 28. Applied Moment-Max Crack Width Comparison for the FRP Experiments to the Grade 60 Controls

Test to Predicted Comparisons

Response 2000 Modeling Approach

Response 2000 was used to compare the moment-curvature relationship of the different specimens tested. A typical bridge deck section was defined as 8.5 in thick, with bottom reinforcement consisting of No. 5 bars and with a clear cover of 2.5 in. The concrete and rebar stress-strain behavior were modeled in the program. To create the stress-strain curve for the rebar, the program uses several input parameters including, elastic modulus, yield strength, strain at yield, strain at onset of strain hardening, ultimate strain, and ultimate stress. Table 13 shows the parameters and their magnitudes entered into Response 2000 that most closely matched the full rebar measured stress-strain curves.

Table 13. Rebar Stress-Strain Inputs to Response 2000

Parameter	Grade 60	ECR	N32	ASTM A1035	UNS S32304	GFRP	BFRP*	CFRP*
Elastic Modulus (ksi)	30000	29000	27000	30000	27000	8000	8000	18500
Yield Stress (ksi)	63	65	76	105	76	145	116**	275
Strain @ on Set of Strain Hardening (με)	7,200	6,500	2,900	3,300	2,900	18,300	14,400**	14,900
Ultimate Stress (ksi)	103	106	110	158	110	145	116**	275
Ultimate Strain (με)	65,000	59,000	110,000	15,000	15,000	18,000	14,400**	14,900

* Properties are dependent of the bar size. No. 5 and No. 3 bars were implemented in the study for BFRP and CFRP, respectively. ** Maximum tensile tress and deformation measured during testing for BFRP due to slipping in the test setup. This value is similar to the guaranteed design tensile strength provided by the manufacturer website (115 ksi) for No. 5 bars.

Moment-Curvature Analysis

The flexural behavior comparison from the conducted experiments to that obtained from a sectional analysis performed in Response 2000 are shown in Figures 29 and 30 for Phase I and Figures 31 and 32 for Phase II specimens. Response 2000 generated moment-curvature trends are consistent with the measured load-deformation response, demonstrating that computer-based sectional analysis tools are a viable and convenient alternative to existing hand solutions when designing with CRR.

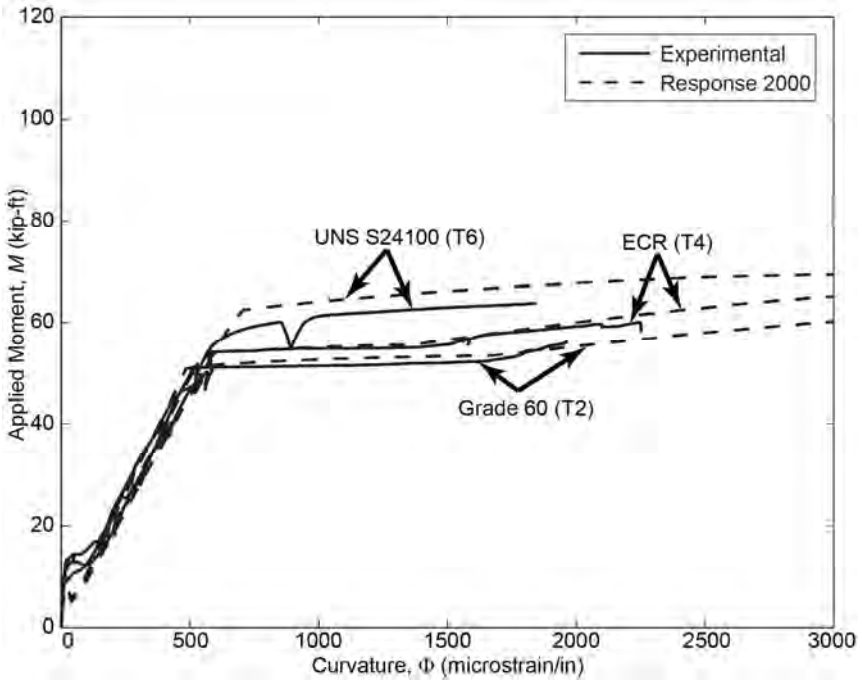

Figure 29. Moment-Curvature Comparison for the Controls Experiments to Response 2000 (Phase I Specimens)

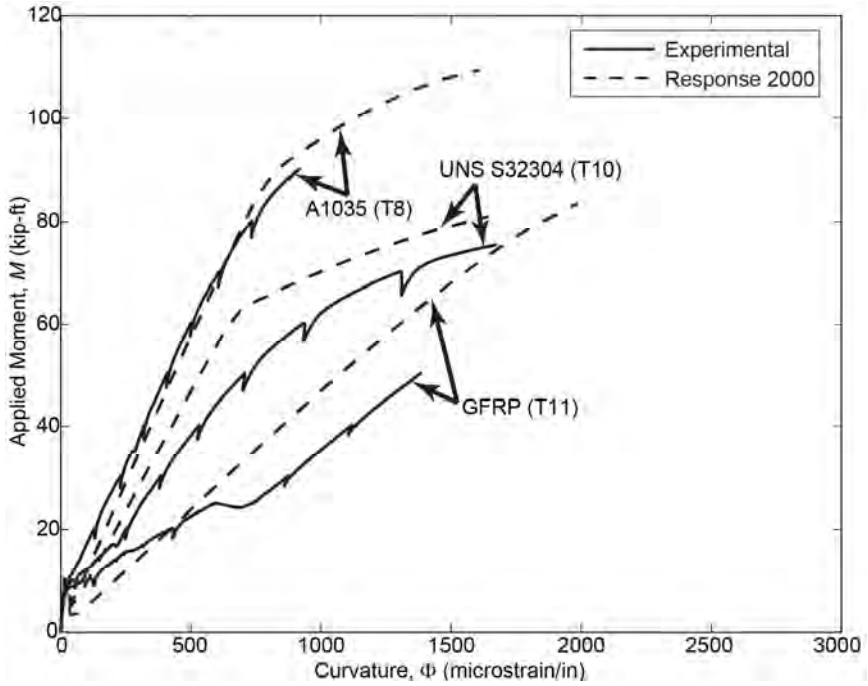

Figure 30. Moment-Curvature Comparison for the One-To-One Replacement Experiments to Response 2000 (Phase I Specimens)

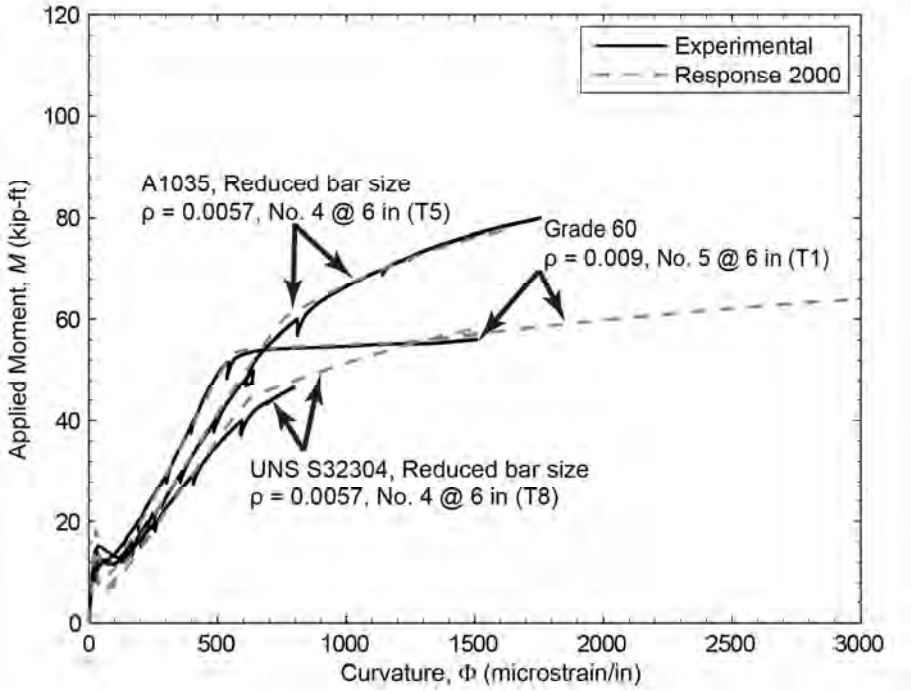

Figure 31. Experimental Moment-Curvature Comparison to Response 2000 Analytical Results for ASTM A1035 and UNS S32304 Specimens (Phase II)

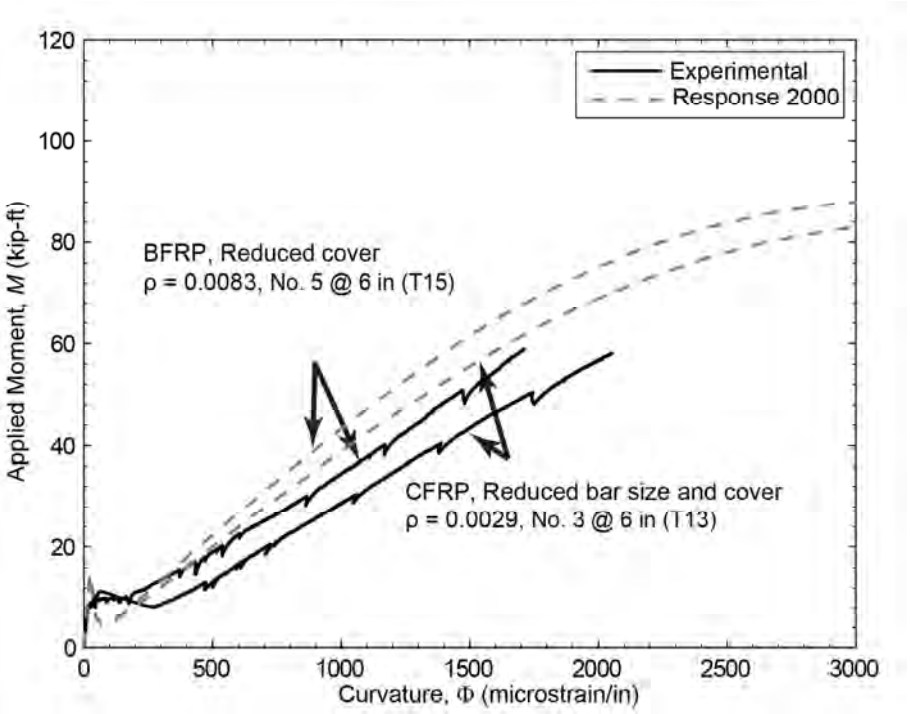

Figure 32. Experimental Moment-Curvature Comparison to Response 2000 Analytical Results for the FRP Specimens (Phase II)

Moment–Crack Width Analysis

Figures 33 through 35 show a comparison of the applied moment versus max crack width relationship from the conducted experiments in Phase II to that obtained from a sectional analysis performed in Response 2000. These results were obtained by assuming no tension stiffening, which lead to values that represent an approximate maximum bound that could be reached and therefore, conservative approximations.

Response 2000 generated applied moment-max crack widths trends that are consistent with the measured response, indicating again that computer-based sectional analysis tools are a feasible and suitable alternative when designing with CRR.

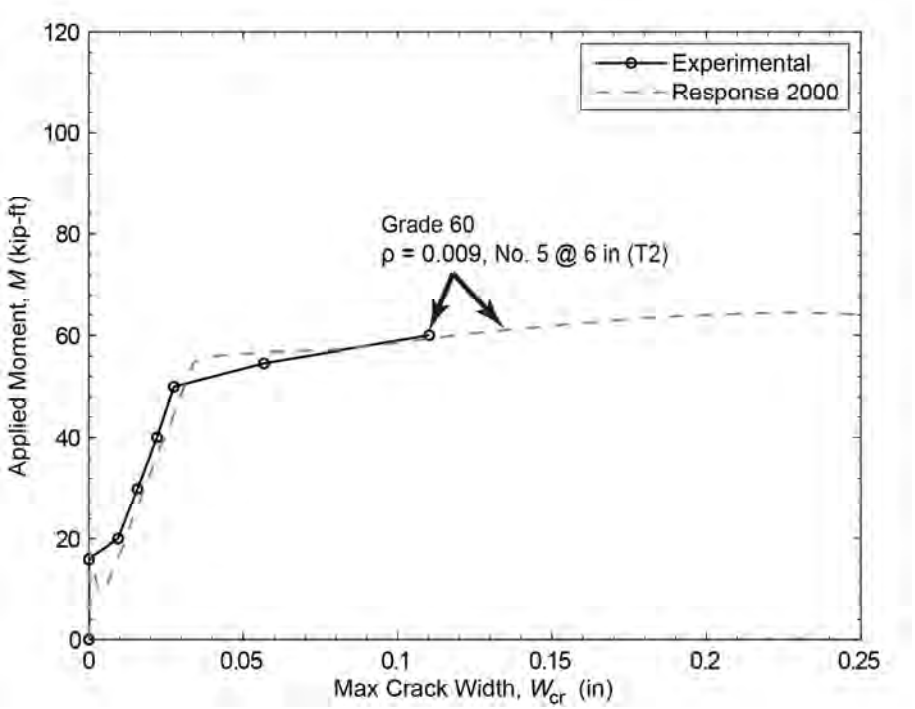

Figure 33. Applied Moment-Max Crack Width Comparison for the Controls Experiments to Response 2000

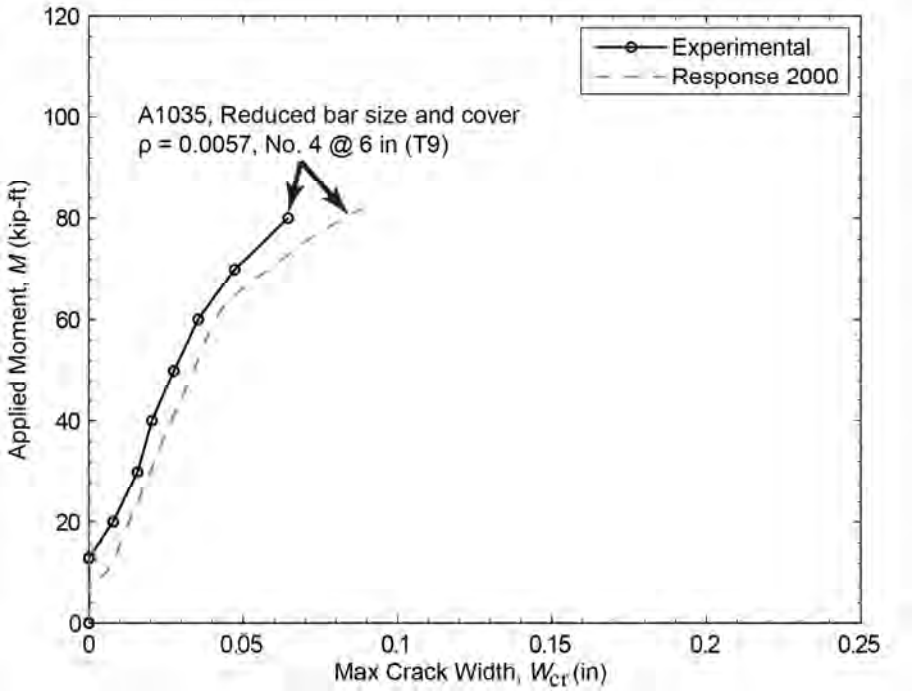

Figure 34. Applied Moment-Max Crack Width Comparison for the ASTM A1035 Experiments to Response 2000

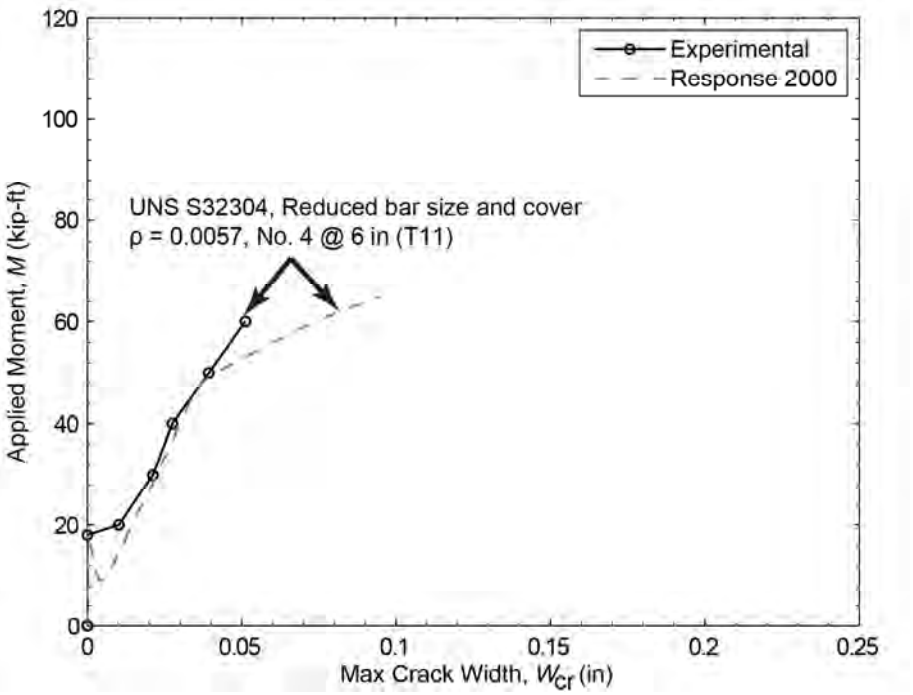

Figure 35. Applied Moment-Max Crack Width Comparison for the UNS S32304 Experiments to Response 2000

Deformability and Ductility Analysis

An essential goal of this study is to begin to contribute ideas to support ongoing research in the ductility-based reinforced concrete design area that can accommodate a wide range of reinforcing material types and stress-strain behavior. This general design framework will be able to accommodate rebar with distinct yield plateaus, gradual yielding, or linear-elastic behavior to failure using computer-based sectional analysis tools like Response 2000. A key component of the framework is design criteria that ensure sufficient deformability and ductility using moment-curvature information.

Ductility ratios such as curvature or deflection at yield to the curvature and deflection at ultimate load are difficult to determine for reinforced concrete that experiences either a gradual yield or no yield at all. A section reinforced with higher strength reinforcement or linear elastic reinforcement (i.e., GFRP) could potentially experience large strains in the reinforcement and thus large curvature and deflection without experiencing a sudden brittle failure. For this reason, the members deformability is defined herein based on the curvature and deflection ratio at M_{test} to the curvature and deflection at $M_{service}$, i.e., $\mu_d = \Delta_{ultimate} / \Delta_{service}$ and $\mu_c = \Phi_{ultimate} / \Phi_{service}$. This is consistent with the deformability-based approach that forms the basis of the ACI provisions for flexural design of reinforced concrete with high strength reinforcement (i.e., Mast et al., 2008).

Tables 14 and 15 provide the ductility ratios, μ_d and μ_c, for each test in Phase I and II, respectively. The midspan deflections $\Delta_{service}$ and $\Delta_{ultimate}$ were measured at the service moment

and the ultimate moment. Since Response 2000 was validated by test results, the midspan curvature $\Phi_{service}$ and $\Phi_{ultimate}$ were found by analyzing each test specimen in Response 2000.

All tests were compared to what is considered an acceptable amount of deformability in a reinforced concrete flexural member according to the ACI and AASHTO specifications (ACI 318-11; AASHTO 2010). This deformability is ensured by exceeding or at least reaching an engineering strain of 0.005 at ultimate load in the rebar. A typical test slab was designed in Response 2000 with the appropriate area of rebar in order for the rebar to have a strain of 0.005 at ultimate load. The slab has a depth of 8.5 in, a width of 36 in, a concrete compressive strength, f'c, of 4000 psi, and reinforcement located at the same depth as the test slabs. For this typical slab μ_c =7.13, which is then used as a deformability limit, i.e., any specimen with μ_c ≥7.13 has acceptable deformability.

Phase I

Table 14. Specimen Deformability (Phase I)

Test Number	Bar Type	Deflection			Curvature		
		$\Delta_{service}$ (in)	$\Delta_{ultimate}$ (in)	$\mu_d = \Delta_{ult.} / \Delta_{ser.}$	$\Phi_{service}$ (microstrain/in)	$\Phi_{ultimate}$ (microstrain/in)	$\mu_c = \Phi_{ult.} / \Phi_{ser.}$
1	Grade 60	0.42	7.07	16.6	238	3537	14.9
2	Grade 60	0.48	8.26	17.2	236	3954	16.7
3	ECR	0.53	6.52	12.3	242	3599	14.8
4	ECR	0.50	5.75	11.6	251	3558	14.2
5	UNS S24100	0.38	6.79	17.8	242	2940	12.2
6	UNS S24100	0.54	6.14	11.4	271	2950	10.9
7	ASTM A1035	0.51	3.60	7.07	211	1804	8.55
8	ASTM A1035	0.54	4.24	7.85	215	1611	7.50
9	UNS S32304	0.64	4.75	7.44	266	1625	6.10*
10	UNS S32304	0.61	5.32	8.72	264	1644	6.23*
11	GFRP	0.96	4.63	4.80	527	1987	3.77*
12	GFRP	0.91	4.00	4.38	580	2188	3.77*
13	ASTM A1035	0.85	3.95	4.65	400	1998	4.98*
14	ASTM A1035	0.87	5.58	6.41	350	2003	5.72*
15	UNS S32304	0.80	5.65	7.09	329	2208	6.71*
16	UNS S32304	0.68	6.04	8.88	310	1780	5.73*
17	ASTM A1035	0.70	5.96	8.52	313	1763	5.62*
18	ASTM A1035	0.70	5.68	8.12	335	1800	5.36*
19	UNS S32304	0.57	4.98	8.70	263	2163	8.22
20	UNS S32304	0.62	5.44	8.77	260	2158	8.28

* μ_c values beneath 7.13, corresponding to 0.005 tensile strain limit for Grade 60 bridge deck.

The average of the two μ_c values for the baseline Grade 60, ECR, UNS S24100, ASTM A1035, UNS S32304, and GFRP tests (T1-T12) were 2.21, 2.03, 1.61, 1.12, 0.86, and 0.52 times this baseline μ_c value for the tension controlled slab, respectively. The two control specimen types that have less deformability than the Grade 60 tension controlled slab were the UNS S32304 and the GFRP, highlighting that these "one-to-one" bridge deck designs may require modifications to ensure equal performance to existing bridges decks at an ultimate limit state.

The average of the two μ_c values for the ASTM A1035 and UNS S32304 reduced bar size experiments (T13-T16) were 0.75 and 0.87 times the calculated baseline μ_c and for the reduced bar size and cover (T17-T20) experiments, 0.77 and 1.16 times respectively. This indicates that, in contrast to a one-to-one bar replacement, a reduction in bar size for the ASTM A1035 and UNS S32304 specimens has less deformability than that of a "typical" Grade 60 bridge deck slab with a rebar strain of 0.005 at ultimate load. The only tested combination that meets the deformability limit is the UNS S32304 reinforced slabs with reduced bar size and reduced cover (T19-T20).

Most of the CRR designs tested in this phase do not meet the ACI and AASHTO ductility requirements. This is because the yield plateau for Grade 60 steel results in large strains at yield, in comparison to the gradually yielding steels (UNS S32304, ASTM A1035) and linear elastic GFRP which experience less strain under load, translating into less curvature and deflection at failure. Tests T19 and T20 considering UNS S32304 stainless steel do give some hope though that sufficient deformability can be achieved, especially if rebar quantity (i.e., the reinforcement ratio ρ) is chosen carefully and clear cover is reduced to keep crack widths tight and service deflections small. The addition of compression steel, not considered in this phase in order to establish a lower bound on flexural performance, also improve ductility. In addition to these ductility limits, it is suggested that some reserve strength be provided in CRR bridge deck slab strip designs, i.e., $M_n \geq 1.2M_u$ where M_n is the nominal flexural strength and M_u is the factored demand moment, to accommodate moment redistribution (softening of the deck over a girder which sheds more moment to midspan in a multi-girder system) at an ultimate limit state. This overstrength is shown to be available in T17-T20 when compared to the Grade 60 control. A more realistic plate analysis of the bridge deck could also be conducted to demonstrate sufficient redundancy for load sharing.

Phase II

Table 15. Specimen Deformability (Phase II)

Test Number	Bar Type	Deflection			Curvature		
		$\Delta_{service}$ (in)	$\Delta_{ultimate}$ (in)	$\mu_d = \Delta_{ult.} / \Delta_{ser.}$	$\Phi_{service}$ (microstrain/in)	$\Phi_{ultimate}$ (microstrain/in)	$\mu_c = \Phi_{ult.} / \Phi_{ser.}$
1	Grade 60	0.48	5.21	10.76	251	3297	13.11
2	Grade 60	0.55	4.54	8.32	252	3308	13.11
3	Grade 60	0.50	3.91	7.77	289	3126	10.84
4	Grade 60	0.45	4.62	10.18	267	2755	10.33
5	ASTM A1035	0.68	4.94	7.23	341	2723	7.98
6	ASTM A1035	0.65	4.46	6.85	311	2407	7.74
7	UNS S32304	0.90	6.37	7.05	381	2913	7.64
8	UNS S32304	0.82	6.61	8.05	402	2955	7.34
9	ASTM A1035	0.53	4.89	9.17	302	2517	8.34
10	ASTM A1035	0.46	4.03	8.73	252	2227	8.84
11	UNS S32304	0.45	4.86	10.70	275	2430	8.85
12	UNS S32304	0.52	5.20	9.98	314	2537	8.07
13	CFRP	1.46	6.17	4.24	647	3254	5.03*
14	CFRP	1.52	6.45	4.23	642	3243	5.05*
15	BFRP	1.24	6.51	5.24	599	3635	6.07*
16	BFRP	1.12	5.96	5.31	596	3623	6.08*

* μ_c values beneath 7.13, corresponding to 0.005 tensile strain limit for Grade 60 bridge deck

The average of the two μ_c values for the baseline Grade 60 single reinforced, Grade 60 double reinforced, ASTM A1035 with 2.50 in clear cover, ASTM A1035 with 2.00 in clear cover, UNS S32304 with 2.5 in clear cover, UNS S32304 with 2.0 in clear cover, CFRP and BFRP were 1.84, 1.48, 1.10, 1.20, 1.05, 1.19, 0.71 and 0.85 times the baseline μ_c value (7.13) for the tension controlled slab, respectively. The only two specimen types that have less deformability than the Grade 60 tension controlled slab were the CFRP and the BFRP.

The 0.5 in decrease in clear cover improves the ASTM A1035 and UNS S32304 specimen ductility by 9% and 13%, respectively. A reduction in rebar size for ASTM A1035 and UNS S32304 specimens resulted in a deformability greater than that of a "typical" Grade 60 bridge deck slab with a 0.005 rebar strain at ultimate load.

CONCLUSIONS

- *For ASTM A1035 and UNS S32304 specimens, a decrease in bar size and clear cover (2.0 in instead 2.50 in) proved to have similar deformability ratios and crack widths that comply with current AASHTO requirements, with as much as 36% less steel. Bridge deck slabs*

employing high strength rebar without a defined yield plateau can still provide ductility consistent with AASHTO and ACI ductility limits at an ultimate limit state.

- *CRR bridge deck designs can be identified that meet current code serviceability and strength requirements, with the added benefit of corrosion resistance, by using programs like Response 2000.*
- *Compression reinforcement should be considered in design calculations to accurately represent ductility and flexural failure mode (i.e., compression or tensile controlled).*
- *The GFRP, BFRP and CFRP specimens had less deformability and experienced larger crack widths at service moment than the Grade 60 control and further consideration is needed to identify a viable bridge deck reinforcing scheme (spacing and bar size) for these bar types.*

RECOMMENDATIONS

1. *VDOT's Structure and Bridge Division should consider reducing the bar size for CRR.* Experimental and analytical results showed that ASTM A1035 and UNS S32304 specimens can be designed such that they provide ductility and serviceability limits consistent with AASHTO requirements as shown in the "Results and Discussion" section. Laboratory testing supports moving forward with a field demonstration project.

2. *VDOT's Structure and Bridge Division should consider decreasing the VDOT concrete cover requirements for bridge deck slabs when using CRR* to improve the serviceability requirements and the flexural capacity. Throughout the experimental program and presented in the "Results and Discussion" section, a 0.5 in reduction in the concrete cover improved the flexural behavior (i.e. flexural capacity, deformability and crack widths) of CRR specimens. Laboratory testing supports moving forward with a field demonstration project.

3. *VDOT's Structure and Bridge Division should work with AASHTO, and VCTIR if needed, to begin assessing the best approach for allowing the use of sectional analysis software, such as Response 2000, to evaluate the strength and serviceability requirements of concrete bridge deck slabs reinforced with CRR in lieu of the current AASHTO method.* Analytical results, such as moment-curvature and moment-crack widths relationships, obtained from this software type proved to be consistent with experimental results as shown in the "Test to predicted comparison" section.

COSTS AND BENEFITS ASSESSMENT

In 1998, the direct cost of corrosion in the United States was $275.7 billion/year, representing approximately 3.14% of the U.S. economy gross domestic product (GDP); from which $29.7 billion/year and $22.6 billion/year were caused by the transportation and infrastructure sectors, respectively (Koch et al., 2002). This influence that corrosion has on the

U.S economy has incentivized several life cycle cost estimations that focus on transportation structures. Nevertheless, these studies often differ one to the other depending on the assumptions made.

The use of corrosion-resistant rebar (CRR) as a solution to decrease the cost of corrosion is a challenge to justify on a first cost basis. However, life cycle cost estimations have opened the door to overcome these obstacles. Table 16 shows the rebar cost per pound of material for CRR (2011-2012 VDOT bids) and Table 17 contains the results of a 100 year life cost analysis. This life cycle cost analysis did not consider crack sealing, deck patching, traffic control and surface preparation for overlays.

In these tables it is shown that even though CRR is two times more costly than Grade 60 rebar on a first cost basis it can actually result in 40% to 45% savings in life cycle costs (base price) and 50% to 70% savings considering a 2% inflation over a 100 years of service life due to minimized repair costs. For a two lane single span bridge, 38 ft. wide and 100 ft. long, this translated into a lower bound savings of approximately $600,000 (base price) and $1,900,000 (2% inflation) in maintenance costs over the life of the bridge.

Table 16. Corrosion-resistant Rebar Cost (2011-2012) (Balakumaran, 2013 Unpublished Data)

Type	Rebar Cost ($/lb)	Rebar Construction Cost ($/yd^2)
Black*	1.01	178.47
Epoxy Coated Rebar (ECR)	1.89	229.68
ASTM A1035**	1.96	233.75
Stainless Steel 316L***	3.13	301.86

*ASTM A615, **ASTM A1035, *** UNS S31603.

Table 17. 100 Year Life Cycle Costs ($/Yd^2) for Concrete Bridge Decks Using CRRs (2011-2012) (Balakumaran, 2013 Unpublished Data)

Concrete Bridge Deck – 100 Year Life Cycle Cost ($/yd2)					
Rebar Type		Black*	ECR	A1035**	316L***
a	Construction Costs	178.47	229.68	233.75	301.86
b	Total Repair/Overlays costs	283.89	227.66	38.40	-
b.1	Overlay @ 1st repair	94.63 SF @ 22.2	94.63 SF @ 36.2	38.40 EPO @ 88	-
b.2	Overlay @ 2nd repair	94.63 SF @ 47.2	94.63 SF @61.2	-&	-
b.3	Overlay @ 3rd repair	94.63& SF @ 72.2	38.40& EPO@ 86.2	-	-
c	100 Year Life Cost (Base Price)	462	457	272	302
d	100 Year Life Cost (2% Inflation)	962	953	453	302
e	Projected Service Life (Years)	97.2	96.2	98	100+

*ASTM A615, **ASTM A1035, *** UNS S31603.
&: No rehabilitations beyond 95 years of service; SF: Silica Fume Overlay 1 ¼" to 1 ¾" (25 year life) + Milling; EPO: Epoxy Overlay (10-year life).

Table 17 shows that the cost related to the implementation of Epoxy rebar are higher than ASTM A1035 and 316L (UNS S31603) as the 100 year life cycle cost of Epoxy rebar is at least 50% higher than the others mentioned. Similarly, another study found that a comprehensive in-place direct cost of Epoxy rebar (that includes the deck sealing operations on concrete decks reinforced with Epoxy rebar, its indirect labor costs and road user costs to the public) are 2.7 to 3.0 times higher than ASTM A1035 (Sharp and Moruza, 2009). In addition, a study concluded that life cycle costs of stainless steel reinforcement were 13% lower than A615 blacks bar for a river crossing highway bridge, the Schaffhausen Bridge (McGurn, 1988). While another investigation determined that ECR was less costly than stainless steel and A615 conventional steel over the life of a bridge deck if its service life could reach 75 years (Ji et al., 2005). Variability in the life cycle cost trends is caused by bridge location, traffic volume, concrete mixture, concrete cover, design and detailing, exposure conditions and others, however looking across the data it is clear that CRR is less costly than Grade 60 rebar over the life of a bridge.

ACKNOWLEDGMENTS

The authors are grateful for the thoughtful guidance and support provided by Deborah Mangiaracina from the Virginia Department of Transportation (VDOT), Michael M. Sprinkel from the Virginia Center for Transportation Innovation and Research (VCTIR), and Rudy Maruri of the Federal Highway Administration. Dennis Huffman and Brett Farmer, lab technicians at Virginia Tech, played an essential role in the fabrication of the CRRs specimens. Also, we are thankful for the excellent work conducted by Virginia Tech graduate students Galo Bowen, Paul Zheng, Valerie Black and Adrian Lorenzoni during this research program. Finally, we really appreciate the excellent work done during the review process by Michael C. Brown, G. Michael Fitch, Jose P. Gomez, Deborah Mangiaracina, Prasad L. Nallapaneni, and Julius F. J. Volgyi, Jr.

REFERENCES

American Association of State Highway and Transportation Officials. *Standard Specifications for Highway Bridges, 16th Edition.* Washington, DC, 1996.

American Association of State Highway and Transportation Officials. *AASHTO LRFD Bridge Design Specifications, 5th Edition*. American Association of State Highway and Transportation Officials, Washington, DC, 2010.

American Association of State Highway and Transportation Officials. *AASHTO MP 18M/MP 18-09: Standard Specification for Uncoated, Corrosion-Resistant, Deformed and Plain Alloy, Billet-Steel Bars for Concrete Reinforcement and Dowels.* Washington, DC, 2010.

American Concrete Institute. ACI Committee 318. *Building Code Requirements for Structural Concrete (ACI 318-11) and Commentary*. Farmington Hills, MI, 2011.

American Concrete Institute. ACI Committee 408. *Bond and Development of Straight Reinforcing Bars in Tension* (ACI 408R-03). Farmington Hills, MI, 2003.

American Concrete Institute. ACI Committee 440. *Specification for Carbon and Glass Fiber-Reinforced Polymer Bar Materials for Concrete Reinforcement* (ACI 440.6-08). Farmington Hills, MI, 2008.

ASTM International. ASTM A370: Standard Test Methods and Definitions for Mechanical Testing of Steel Product. *In Annual Book of ASTM Standards, Vol. 01.03: Steel Plate, Sheet, Strip, Wire; Stainless Steel Bar.* West Conshohocken, PA, 2005.

ASTM International. ASTM A955/A955M: Standard Specification for Deformed and Plain Stainless-Steel Bars for Concrete Reinforcement. *In Annual Book of ASTM Standards, Vol. 01.04: Steel Structural, Reinforcing, Pressure Vessel, Railway.* West Conshohocken, PA, 2011.

ASTM International. ASTM A1035/A1035M: Standard Specification for Deformed and Plain, Low-carbon, Chromium, Steel Bars for Concrete Reinforcement. *In Annual Book of ASTM Standards, Vol. 01.04: Steel Structural, Reinforcing, Pressure Vessel, Railway.* West Conshohocken, PA, 2011.

ASTM International. ASTM C143: Standard Test Method for Slump of Hydraulic-Cement Concrete. *In Annual Book of ASTM Standards, Vol. 04.02: Concrete and Aggregates.* West Conshohocken, PA, 2010b.

ASTM International. ASTM C192: Standard Practice for Making and Curing Concrete Test Specimens in the Laboratory. *In Annual Book of ASTM Standards, Vol. 04.02: Concrete and Aggregates.* West Conshohocken, PA, 2007.

ASTM International. ASTM C231: Standard Test Method for Air Content of Freshly Mixed Concrete by the Pressure Method. *In Annual Book of ASTM Standards, Vol. 04.02: Concrete and Aggregates.* West Conshohocken, PA, 2010c.

ASTM International. ASTM C496: Standard Test Method for Splitting Tensile Strength of Cylindrical Concrete Specimens. *In Annual Book of ASTM Standards, Vol. 04.02: Concrete and Aggregates.* West Conshohocken, PA, 2004.

ASTM International. ASTM C1064: Standard Test Method for Temperature of Freshly Mixed Hydraulic-Cement Concrete. *In Annual Book of ASTM Standards, Vol. 04.02: Concrete and Aggregates.* West Conshohocken, PA, 2008.

Bentz, E.C. *Sectional Analysis of Reinforced Concrete*. Ph.D. Dissertation, University of Toronto, Ontario, Canada, 2000.

Clemena, G., Kukreja, D., and Napier, C. *Trial Use Of A Stainless Steel-Clad Steel Bar In A New Concrete Bridge Deck In Virginia.* VTRC 04-R5. Virginia Transportation Research Council, Charlottesville, 2003.

Gurlanick, S. High-Strength Deformed Steel Bars For Concrete Reinforcement. *ACI Journal Proceedings*, Vol. 57, No. 9, 1960, pp. 241-282.

Faza, S., Kwok, J., and Salah, O. *Concrete High-Rise Construction*. Council on Tall Buildings and Urban Habitat, Chicago, Illinois, 2008.

Hartt, W. H., Powers, R. G., Leroux, V., and Lysogorski, D. K. *Critical Literature Review of High-Performance Corrosion Reinforcements in Concrete Bridge Applications*. FHWA-HRT-4-093. Federal Highway Administration, Washington, DC, 2004.

Hognestad, E., Winter, G., Mavis, F.T., and Greaves, M. J. High-Strength Reinforcing Steels for Concrete Bridges. In *Transportation Research Record: Journal of the Transportation Research Board,* No. 39. Transportation Research Board of the National Academies, Washington, DC, 1960, pp. 103-119.

Ji, J., Darwin, D., and Browning, J. *Corrosion Resistance of Duplex Stainless Steels and MMFX Microcomposite Steel for Reinforced Bridge Decks*. SM Report No. 80. The University of Kansas Center for Research, Inc., Lawerence, Kansas, 2005.

Koch, G.H., Brongers, M.P.H., Thompson, N.G., Virmani, Y.P., and Payer, J.H. *Corrosion Costs and Preventative Strategies in the United States,* FHWA-RD-01-156. Federal Highway Administration, Washington DC, 2002

Malhas, F.A. *Preliminary Experimental Investigation of the Flexural Behavior of Reinforced Concrete Beams using MMFX Steel.* Final Report for MMFX Technologies Corporation, University of North Florida, Jacksonville, Florida, 2002.

Mast, R.F., Dawood, M., Rizkalla, S.H., and Zia, P. Flexural Strength Design of Concrete Beams Reinforced with High-Strength Steel Bars. *ACI Structural Journal*, Vol. 105, No. 5, 2008, pp. 570-577.

McGurn, J.F. *Stainless Steel Reinforcing Bars in Concrete.* Nickel Development Institute, Toronto, Ontario, Canada,1988.

Moncarz, P.D., and Krawinkler, H. *Theory and Application of Experimental Model Analysis in Earthquake Engineering*. Report No. 50. John A. Blume Earthquake Engineering Research Center, Standford, California, 1981.

Sarver, B. *Mechanical and Geometric Properties of Corrosion-Resistant Reinforcing Steel in Concrete*. MS Report. Virginia Tech, Blacksburg, Virginia, 2010.

Seliem, H.M., Lucier, G., Rizkalla, S.H., and Zia, P. Behavior of Concrete Bridge Decks Reinforced with High-Performance Steel. *ACI Structural Journal*, Vol. 105, No. 1, 2008, pp. 78-86.

Shahrooz, B.M., Reis, J., Wells, E., Miller, R.A., Harries, K., and Russell, H.G. Flexural Behavior and Design with High-Strength Bars and Those without Well-Defined Yield Point. In *Transportation Research Record: Journal of the Transportation Research Board.* Transportation Research Board of the National Academies, Washington, DC, Vol. 10, 2010, pp. 103-111.

Sharp, S.R., and Moruza, A.K. *Field Comparison of the Installation and Cost of Placement of Epoxy-Coated and MMFX 2 Steel Deck Reinforcement: Establishing a Baseline for Future Deck Monitoring.* VTRC 09-R9. Virginia Transportation Research Council, Charlottesville, 2009.

Torok, M., Golparvar-Fard, M., and Kochersberger, K. Post-Disaster Robotic Building Assessment: Automated 3D Crack Detection from Image-based 3D Reconstructions. In *Proceedings of the 2012 ASCE International Conference on Computing in Civil Engineering,* Clear Waters, Florida, 2012, pp, 397-404.

Virginia Department of Transportation. *Road and Bridge Specifications*. Richmond, 2007.

Virginia Department of Transportation. *Modifications to the AASHTO LRFD Bridge Design Specification*s, 5th Edition. Richmond, 2010.

Virginia Department of Transportation. *Manuals of the Structure and Bridge Division–Volume V Series*. Richmond, 2011.

Yotakhong, P. *Flexural Performance of MMFX Reinforcing Rebars in Concrete Structures*. M.S. Thesis, North Carolina State University, Raleigh, North Carolina, 2003.

Zahavi, V., and Ryan, J.M. Stability of Travel Over Time. *In Transportation Research Record: Journal of the Transportation Research Board*, No. 750. Transportation Research Board of the National Academies, Washington, DC, 1980, pp. 250-263.

Zheng, P., and Moen, C.D. *Crack Detection and Measurement Utilizing Image-Based Reconstruction.* SEM-14-01. Virginia Tech, Civil and Environmental Engineering Department, Blacksburg, 2014.